



Tectonic and climatic significance of Oligocene-Miocene eolian sandstones in the Andean foreland basin of Argentina

Daniel Starck^{a,*}, Tomas N. Capaldi^b, Facundo Fuentes^c, Brian K. Horton^d

^a Independent Consultant, La Plata, Argentina

^b Scripps Institution of Oceanography, University of California, San Diego, La Jolla, CA, USA

^c YPF, 515 Macacha Güemes, Buenos Aires, Argentina

^d Institute for Geophysics and Department of Earth and Planetary Sciences, Jackson School of Geosciences, University of Texas at Austin, Austin, TX, USA

ABSTRACT

Late Oligocene-early Miocene aridification in the retroarc foreland basin adjacent to the southern central Andes was recorded by widespread eolian conditions that coincided with accelerated subsidence driven by the main phase of Andean tectonic loading. An extensive eolian dune system, which is rare in most foreland basins, indicates specific conditions in terms of climate (aridity), atmospheric circulation, orography, sediment sources, dispersal patterns, and accommodation space. Detrital zircon U-Pb geochronological results for eolian sandstones spanning 20 foreland localities in northwestern to west-central Argentina, from 22°S to 36°S, reveal relatively localized Andean sources rather than regional cratonic provenance. Clastic detritus was largely derived from Phanerozoic igneous and sedimentary rocks of the Andean magmatic arc and retroarc fold-thrust belt during initial shortening-induced uplift of hinterland regions such as the Western Cordillera, Principal Cordillera, and Frontal Cordillera. This provenance record provides the earliest evidence for major westerly winds, transporting Andean detritus broadly eastward to the foreland basin (with common axial northward deflections) during a climate shift marked by the latest Oligocene-earliest Miocene inception of arid conditions. In addition to the climatic implications, independent stratigraphic data provide the basis for a compilation of sediment accumulation histories showing that eolian deposition was synchronous with accelerated subsidence attributable to enhanced Andean shortening. We propose that accelerated Andean uplift in the latest Oligocene-early Miocene generated rain-shadow conditions contemporaneous with increased sediment accommodation in the foreland basin, underscoring the important influence of tectonic processes on regional climate.

1. Introduction

Eolian depositional systems present valuable opportunities to understand climatic, tectonic, and paleogeographic conditions during nonmarine basin evolution. Fundamentally, eolian systems require specific climatic scenarios involving low-precipitation and semiarid to hyperarid conditions. However, the establishment and long-term preservation of eolian systems in the rock record may have further implications for continental paleogeography, atmospheric circulation, weather patterns, sediment provenance dynamics, mountainous topography, and the creation of sediment accommodation space. In particular, tectonic processes are important in defining the orographic effects on prevailing winds, the position and scale of sediment source areas, the surface exposure of source rock materials, and the regional subsidence necessary for sediment deposition and preservation.

Foreland basins form in active tectonic settings adjacent to large contractional orogenic belts. Along convergent plate margins, high topography within the subduction-related magmatic arc and retroarc fold-thrust belt provides sources of sediment and may form orographic

barriers that guide regional wind patterns and generate rain shadows within the adjacent foreland basin. Nevertheless, sustained eolian systems are rare in most nonmarine foreland basins, which tend to be dominated by fluvial or megafan deposition (Horton and DeCelles, 2001; Leier et al., 2005; Hartley et al., 2010). Reports of large-scale eolian deposition in foreland settings commonly involve uncertainties over the tectonic, accommodation, and provenance configurations (e.g., Bjerrum and Dorsey, 1995; Allen et al., 2000; Starck and Anzótegui, 2001; Tripaldi and Limarino, 2005; Coutand et al., 2006; Carrapa et al., 2012; Capaldi et al., 2019; Garzanti et al., 2022).

In South America, an extensive eolian succession marks a pivotal shift in the Cenozoic evolution of the retroarc foreland basin adjacent to the southern central Andes. In northern to central Argentina (Fig. 1), the latest Oligocene to earliest Miocene defines a change from slowly subsiding or isolated subbasins to a contiguous regional foreland basin. Corresponding basin fill is mostly associated with deposition of mud, sand, and gravel in ephemeral (overbank) fluvial, braided fluvial, fluvial megafan, and alluvial fan environments (Jordan and Alonso, 1987; Jordan et al., 1993, 1996, 2001; Limarino et al., 2001; Vergés et al.,

* Corresponding author.

E-mail address: daniel@starck.im (D. Starck).

2001; Siks and Horton, 2011; Levina et al., 2014). However, a remarkable belt of eolian sandstones is distributed extensively along the eastern flank of the Andes between 22°S and 36°S (Fig. 1).

Despite the difficulties in dating these non-fossiliferous eolian

deposits, geochronological evidence data point to a principally ~24–16 Ma age range spanning the latest Oligocene through early Miocene (Fig. 2) (Dávila and Astini, 2007; Zambrano et al., 2011; del Papa et al., 2013a, 2013b; Ciccioli et al., 2014a; Levina et al., 2014; Horton et al.,

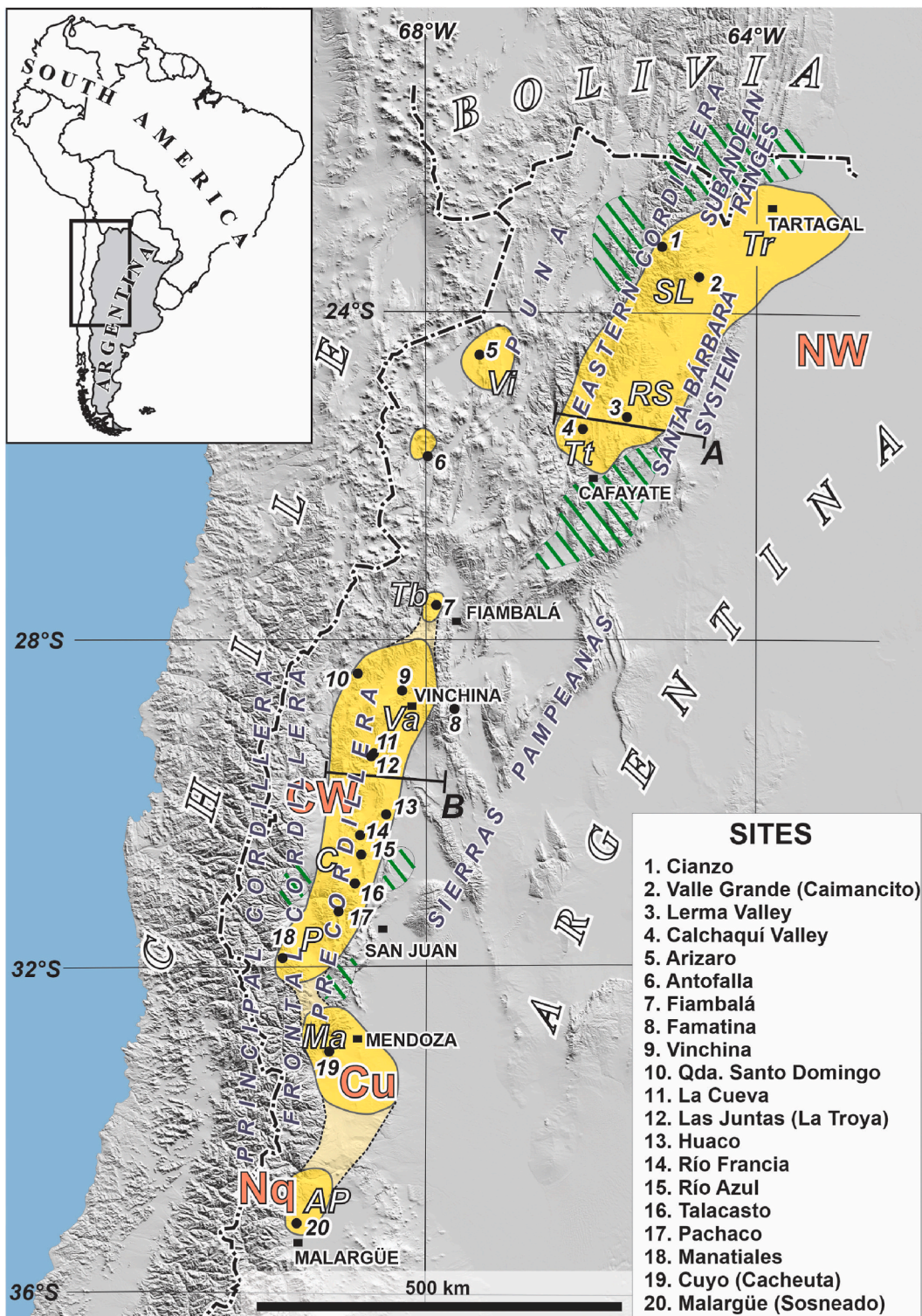


Fig. 1. Shaded relief map of the southern central Andes and adjacent retroarc foreland basin of northern and central Argentina showing zones with eolian basin fill (yellow shading), inferred connections (light yellow shading), and no eolian deposits (green ruled pattern). Representative stratigraphic sections are defined for foreland Sites 1–20 (Figs. 2–4), with schematic stratigraphic cross sections for basin transects (A) ~25.5°S and (B) ~30°S (Figs. 5 and 6). Basin segments include: (1) NW: northwest; (2) CW: west-central; (3) Cu: Cuyo; (4) Nq: Neuquén. Major eolian units include: Tr: Tranquitas Formation; SL: San Lorenzo Formation; Vi: Vizcachera Formation; RS: Río Seco Formation; Tt: Tintín member of Angastaco Formation; Tb: Tambaré Formation; Va: Vallecito Formation; C: Cuculí Formation; P: Pachaco Formation; Ma: Mariño Formation. AP: Agua de la Piedra Formation.

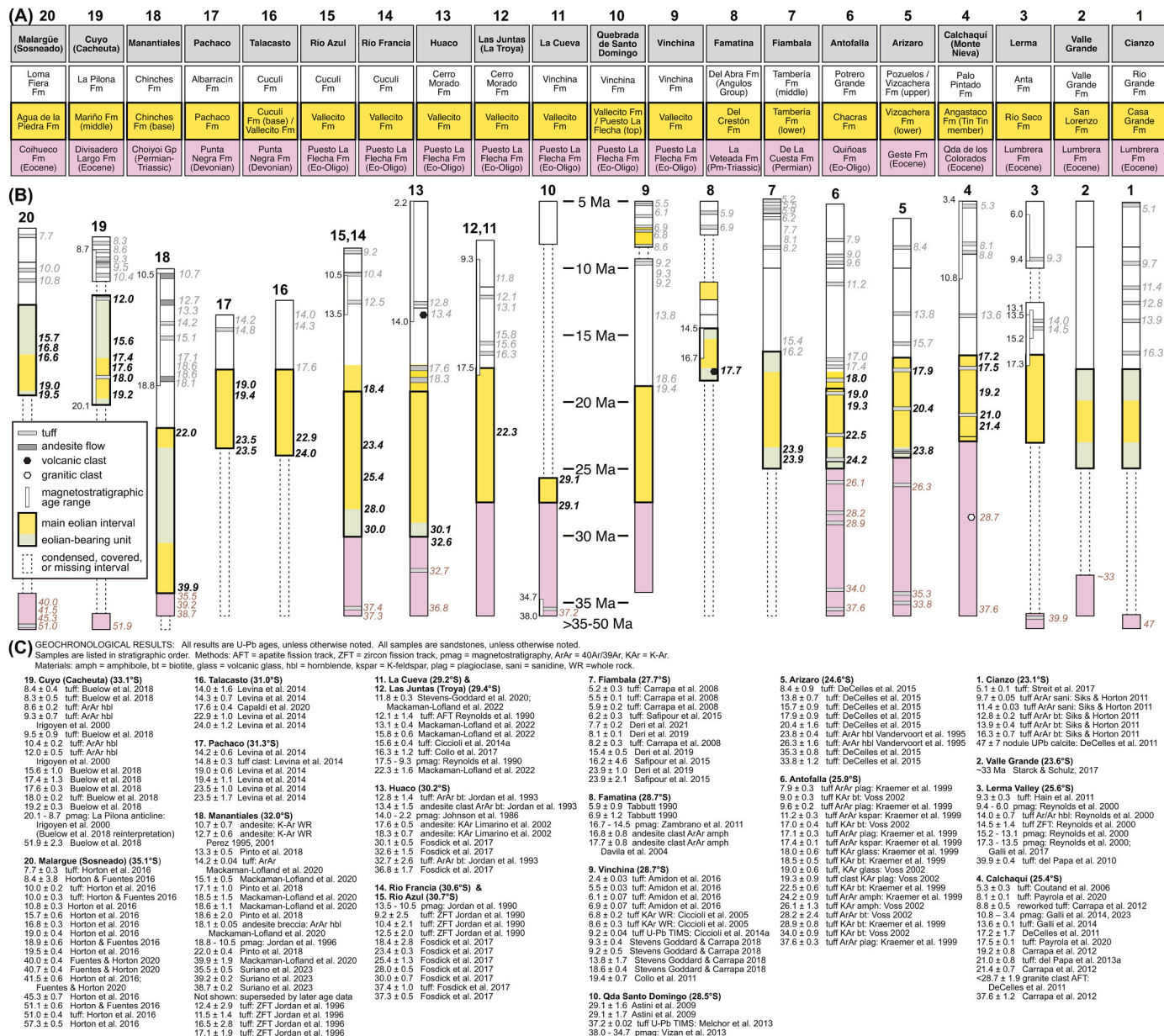


Fig. 2. Stratigraphic profiles and radiometric age constraints for eolian-bearing Cenozoic successions from 20 localities in the Andean foreland basin of northern and central Argentina. Stratigraphic charts (above) and vertical profiles (below) show the principal eolian units, underlying and overlying units, available age constraints, and corresponding references.

2016; Fosdick et al., 2017; Reat and Fosdick, 2018; Capaldi et al., 2020). The regional synchronicity and comparable stratigraphic position at the base of a thick synorogenic succession suggest that distinct sedimentary, tectonic, and/or climatic conditions prevailed for a ~1500 km N-S distance along the basin axis. This eolian record coincided with accelerated Andean crustal shortening, raising questions about how eolian processes may be related to tectonic, topographic, and climatic forcings, with further interactions among weathering, erosion, and transport in an arid climate, as well as competition between sediment supply and basin subsidence.

In this study, we report on widespread eolian sedimentation within the Andean retroarc foreland basin of northern and central Argentina. Past studies have identified middle to late Cenozoic eolian deposits over various segments of the foreland basin (e.g., *Candiani et al.*, 2011; *Dávila et al.*, 2004; *Furque et al.*, 2003; *Milana*, 1993; *Starck and Vergani*, 1996; *Pérez*, 2001; *Starck and Anzótegui*, 2001; *Tripaldi and Limarino*, 2005; *Dávila and Astini*, 2003; *Marengo et al.*, 2019; *Ciccioli*

et al., 2023). Here we present an integrated view of the stratigraphic distribution, provenance, and significance of the principal eolian units. The areal distribution and time interval of eolian deposition may indicate an important climatic phase possibly triggered by global climatic variations or regional tectonic activities associated with deformation advance and topographic growth of the Andes mountains. The purpose of this paper is to provide a perspective on uppermost Oligocene-lower Miocene eolian conditions in the context of the Andean foreland basin, synthesize available age constraints and stratigraphic correlations, and present information about provenance and sediment accommodation.

2. Geologic framework

The Andean retroarc foreland basin is the product of flexural subsidence driven by shortening and thickening of South American continental lithosphere. Initial mountain building is commonly linked to accelerated westward motion of the South America plate (e.g., Coney

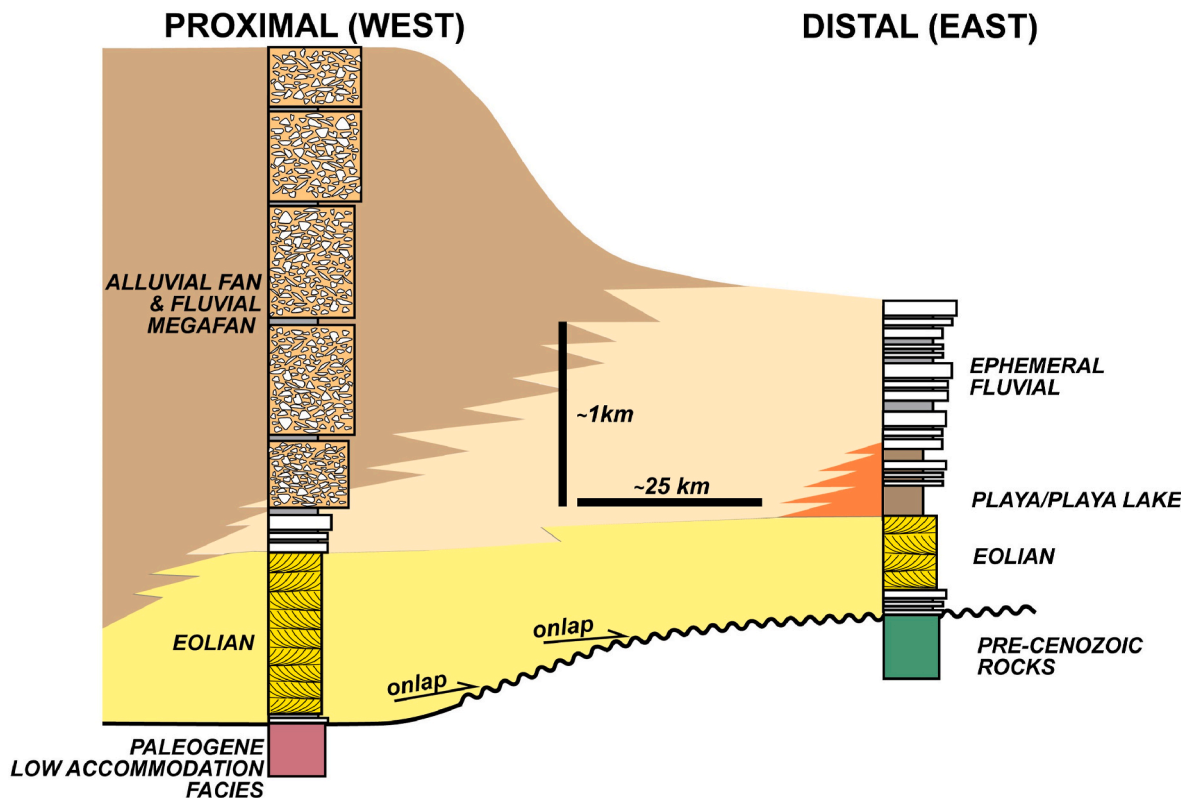


Fig. 3. Idealized stratigraphic profiles of proximal and distal settings of the retroarc foreland basin adjacent to the southern central Andes. Although both profiles show upward coarsening, note the lateral variations in thickness, facies, and depositional systems, with eolian deposits showing considerable lateral continuity.

and Evenchick, 1994; Maloney et al., 2013; Horton, 2018a), as recorded by the Late Cretaceous activation of an incipient fold-thrust belt in far-western segments of the Andean orogenic system. The zone of early Andean shortening and its corresponding foreland basin have been largely overprinted or removed by later deformation, magmatism, and erosion. Such a fragmentary structural and stratigraphic record has led to considerable discussion over the timing and controls on pre-Neogene deformation and basin development (Boll and Hernández, 1986; Jordan and Alonso, 1987; Yrigoyen, 1993; Jordan et al., 1993, 2001; Ramos, 1999; Starck, 2011; DeCelles et al., 2011; Siks and Horton, 2011; del Papa et al., 2013a, 2013b; Fosdick et al., 2017; Horton, 2018b; Capaldi et al., 2020; Giambiagi et al., 2022; Mackaman-Lofland et al., 2022).

Although debate persists over early Andean orogenesis, there is broad consensus that principally Neogene-age structures and nonmarine strata recorded the main phase of Andean shortening and sediment accumulation in the flexural foreland basin spanning northern and central Argentina (Figs. 1 and 2). Along a well-known orogenic transect at 30–32°S (Fig. 3), an earliest Miocene onset of enhanced shortening is consistent with the activation of thrust and reverse faults in the Principal Cordillera along the Chile-Argentina border and the eastward-adjacent Frontal Cordillera (Ramos et al., 1996, 2002; Pérez, 2001). These faults accommodated E-W shortening and commonly reactivated pre-existing normal faults originally formed during earlier extension of Triassic-Jurassic and late Eocene-Oligocene age (Ramos, 1996; Cris-tallini and Ramos, 2000; Giambiagi et al., 2003; Mackaman-Lofland et al., 2019, 2020).

The tectonic history recorded in the west-central segment of the foreland basin at 28–32°S (Fig. 1, CW basin segment) is matched by similar patterns to the north and south. To the north, in northwestern Argentina at 22–26°S (Fig. 1, NW basin segment), early Andean shortening in the western Andes, including the Western Cordillera and Puna plateau, was followed by the main phase of shortening farther east in the Eastern Cordillera, Santa Barbara system, and Subandean Zone (Hain-

et al., 2011; Kley and Monaldi, 2002; Coutand et al., 2006; Starck, 2011; Siks and Horton, 2011; DeCelles et al., 2011, 2015; del Papa et al., 2010, 2013a, 2013b, 2021; Giambiagi et al., 2022). To the south, in western Argentina at 33–36°S, the Cuyo and Neuquén regions (Fig. 1, Cu and Nq basin segments) contain records of limited shortening accommodated within narrow fold-thrust systems defined by hybrid thin- and thick-skinned geometries with common inversion structures (Ramos et al., 1996; Giambiagi et al., 2012; Boll et al., 2014; Fuentes et al., 2016; Horton et al., 2016).

These basin segments (Fig. 1, CW, NW, Cu, and Nq) form part of an integrated retroarc foreland basin containing a 2–4 km thick stratigraphic succession that recorded cratonward advance of proximal western and distal eastern basin margins. This succession is considered for 20 localities, hereafter referred to as Sites 1–20 (Fig. 2). Nearly all parts of the basin express an upward coarsening package (Fig. 3) indicative of progradational clastic facies belts, from distal to proximal depositional settings. Although initially developed as a contiguous feature, the foreland basin has been compartmentalized by subsequent shortening in the fold-thrust belt (e.g., Siks and Horton, 2011; Levina et al., 2014) and intraplate regions such as the Santa Barbara system and Sierras Pampeanas (Ramos et al., 2002; Horton et al., 2022a, 2022b). This structural disruption of the original basin has exposed basin fill in multiple positions in orogen-parallel (N-S) and orogen-normal (E-W) transects. Where sufficient exposure and age control exists, individual facies belts can be traced from the older western components to progressively younger eastern counterparts (e.g., Capaldi et al., 2020).

The Neogene-Quaternary record is dominated by nonmarine clastic facies (Fig. 3). Volumetrically, most depocenters consist of sandy braided fluvial and muddy ephemeral fluvial deposits, with subordinate conglomeratic alluvial fan and fluvial megafan deposits in proximal western localities. Eolian facies are limited to lower stratigraphic levels but span a ~1500 km distance along the basin axis. These eolian deposits, which constitute a wide range of named stratigraphic units

(Fig. 2), share a principally latest Oligocene-early Miocene age and overall stratigraphic position (a) conformably over Paleogene strata that accumulated under slow subsidence regimes or, alternatively, (b) above a basal unconformity over Mesozoic or Paleozoic units. Upsection, eolian facies are typically replaced by progradational fluvial and alluvial fan deposits (Figs. 2–4).

The eolian stratigraphic packages display a large geographic distribution, potentially $>100,000 \text{ km}^2$, from 22°S to 36°S (Fig. 1). Although the duration likely varied locally, most available age control suggests up to 8 Myr of prolonged desert conditions coeval over large areas during the early evolution of the Neogene foreland basin. The areal distribution of desert conditions suggests that eolian facies were developed over a range of different structural settings in the Andean foreland, with some localities situated in proximal realms and others distal to the topographic front of the Andean fold-thrust belt.

Despite the regional coherence of uppermost Oligocene-lower Miocene eolian packages (Fig. 2), anomalous zones of locally older and younger eolian deposition occurred in several restricted areas. This includes eolian deposits of probable late Eocene-early Oligocene age in the Manantiales basin at 32°S (Site 18 Areniscas Chocolate unit; Pinto et al., 2018; Mackaman-Lofland et al., 2020; Suriano et al., 2023) and in the northern Bermejo basin at 29 – 31°S (within the Puesto La Flecha Formation at Sites 10–15; Fosdick et al., 2017; Limarino et al., 2002, 2016; Reat and Fosdick, 2018), as well as late Miocene eolian units in the Vinchina-Quebrada Santo Domingo areas at 28 – 29°S (Sites 9–10) Santo Domingo and Toro Negro Formations; Astini et al., 2009; Dávila and Astini, 2003, 2007; Ciccioli et al., 2014b; Marengo et al., 2019).

3. Sedimentology and stratigraphy

The stratigraphic and sedimentologic framework for upper Oligocene-lower Miocene eolian deposits reflects common features across 20 localities within the retroarc foreland basin of Argentina (Figs. 1–3, Sites 1–20). Analysis of several key stratigraphic sections (Fig. 4) and assessments of depositional processes illustrate the eolian depositional record in the context of precursor basin conditions and the ensuing main phase of foreland basin accommodation. The data span many localities (including type sections of individual formations) in central and northern Argentina from $\sim 22^\circ\text{S}$ to 36°S . Sediments were deposited in a contiguous foreland basin, with a representative E-W (orogen-normal) stratigraphic profile (Fig. 3) that is reflected by specific units defined for stratigraphic sections at $\sim 26^\circ\text{S}$ (Figs. 5, 6A) and $\sim 30^\circ\text{S}$ (Fig. 6B). For simplicity we present the stratigraphic and sedimentologic information according to different segments of the basin from north to south (Fig. 1, NW, CW, Cu, and Nq basin segments).

3.1. Northwest Argentina

The northwestern basin segment (22 – 26°S) contains thick sections of Cenozoic foreland basin fill exposed in the Eastern Cordillera, Santa Barbara system, and Subandean Zone (Fig. 1). Although part of an originally contiguous basin, these deposits are currently exposed in disconnected valleys, which has led to a complex lithostratigraphic nomenclature for the Salta, Tucumán, and Jujuy provinces of Argentina (Fig. 2, Sites 1–6). Nevertheless, the deposits can be placed in an integrative perspective involving two components (Fig. 3): (A) a thin but regionally extensive package of early foreland basin fill and (B) an overlying thick package of coarse-grained deposits representing the

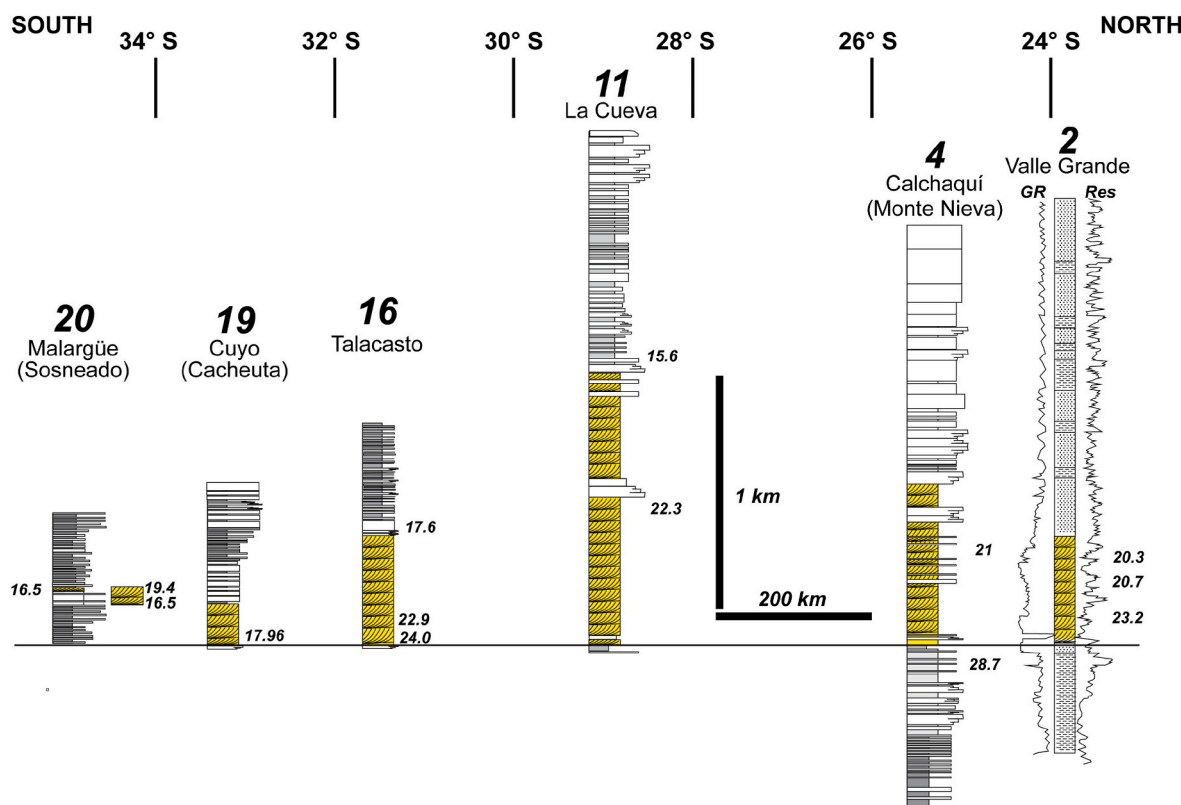


Fig. 4. A series of stratigraphic sections and depositional ages for the retroarc foreland basin adjacent to the southern central Andes, levelled at the base of the eolian stratigraphic interval (yellow shading). Note the lateral variations in the thicknesses of eolian deposits and the host succession. Stratigraphic sections (localities shown in Figs. 1 and 2): Site 2: Valle Grande oil well (Grosso et al., 2013). Site 4: Monte Nieva, Calchaquí Valley (Starck and Vergani, 1996; DeCelles et al., 2011). Sites 11–12: La Cueva-Las Juntas (Tripaldi, 2012; Ciccioli et al., 2014a). Site 16: Talacasto (Levina et al., 2014); Site 19: Cuyo-Cacheuta (Irigoyen et al., 2000). Site 20: Malargüe-Sosneado (Horton et al., 2016).

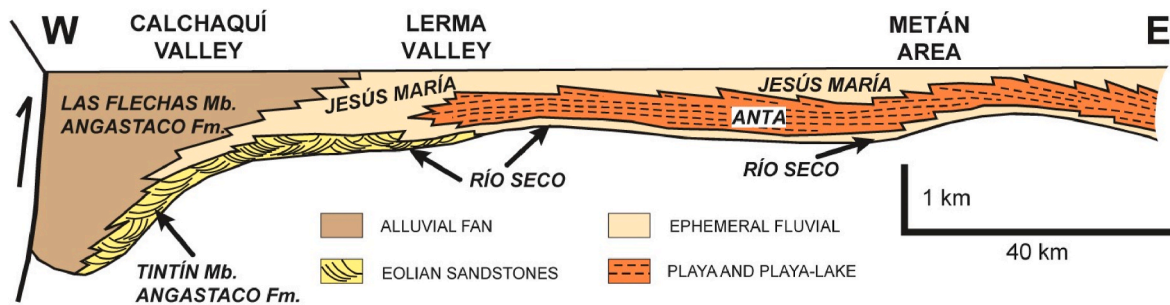


Fig. 5. Stratigraphic profile at $\sim 25.5^{\circ}\text{S}$ depicting contrasting facies and depositional systems within the northwestern basin segment (Sites 3–4) of the retroarc foreland of the southern central Andes. Eolian deposits are limited to lowermost basin fill in proximal to medial settings. Note the dominance of coarse-grained alluvial-fan/fluvial deposits in proximal (western) settings and restriction of playa lake deposits to more distal (eastern) settings. Modified from Starck and Vergani (1996) and Starck and Anzótegui (2001).

main phase of sediment accumulation.

The early foreland basin fill is of chiefly Eocene-Oligocene age and consists of an upward coarsening succession of generally purple to brick-red facies dominated by mudrock deposited in distal fluvial environments, principally overbank settings with considerable pedogenic development, with local lacustrine environments (DeCelles et al., 2011; del Papa et al., 2013a, 2013b). Upsection, the overlying thick package of sandstone and conglomeratic facies defines continued latest Oligocene to Quaternary accumulation in more proximal sectors of the foreland basin (Hernández et al., 1996, 2005; Reynolds et al., 2001; Echavarria

et al., 2003; Calle et al., 2018).

The upper stratigraphic package recorded large-scale eastward advance of the foreland basin, with progradation of fluvial, fluvial megafan, and alluvial fan depositional systems over precursor eolian deposits (Fig. 4, Sites 2–3). In northernmost Argentina, eolian facies occupy the base of the progradational succession, as represented in the Cianzo syncline (Site 1, 23.1°S) and correlative Tres Cruces succession by the lower Casa Grande Formation (Figs. 1 and 2; Boll and Hernández, 1986; Siks and Horton, 2011), and the Valle Grande area (Site 2, 23.6°S) by the San Lorenzo Formation or “Areniscas de Garganta” (Rosario et al.,

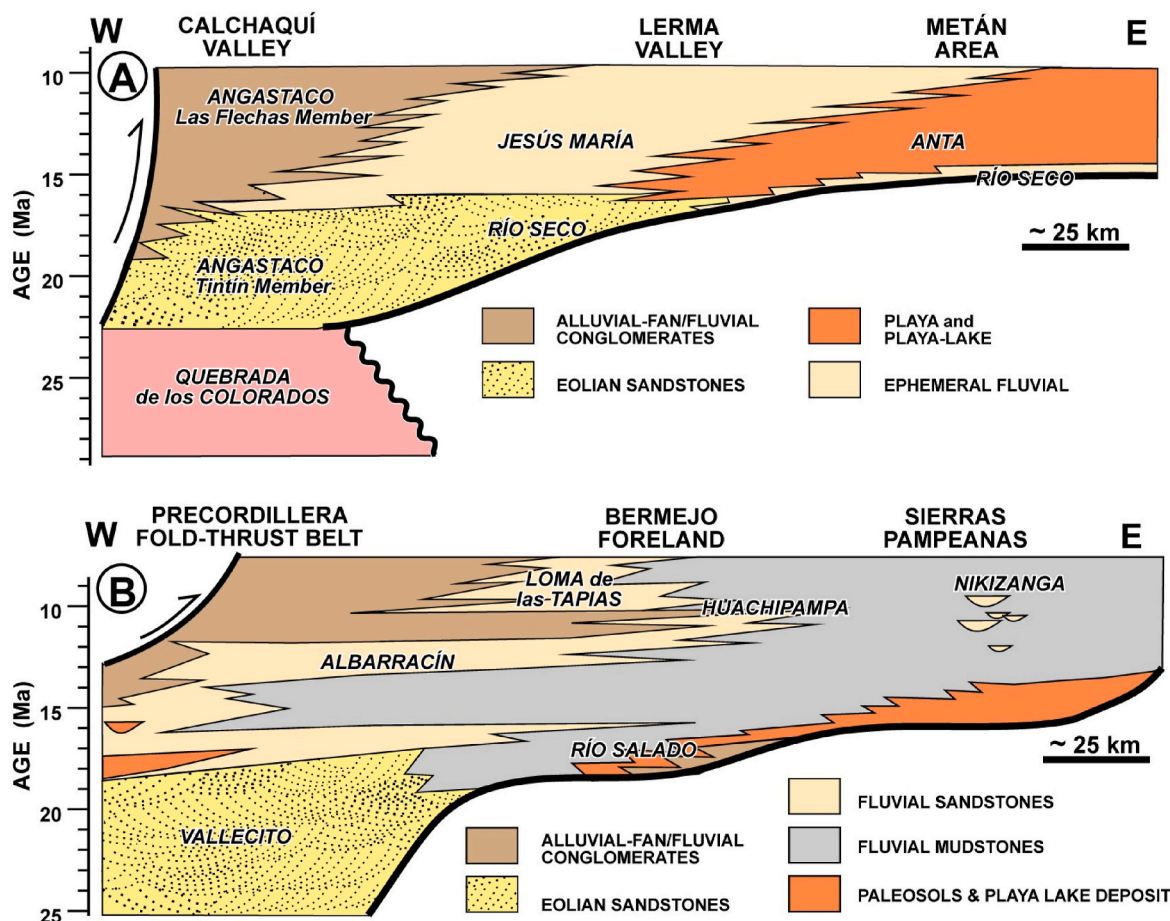


Fig. 6. Schematic time-stratigraphic cross sections for orogen-normal E-W transects across the retroarc foreland basin (A) at $\sim 26^{\circ}\text{S}$ (modified from Starck and Vergani, 1996) and (B) at $\sim 30^{\circ}\text{S}$ (modified from Horton et al., 2022a,b). The sections show different depositional facies (colors) and stratigraphic units (labels), with eolian deposits restricted to lowermost basin fill in proximal to medial settings. Note the upward coarsening and progressive advance (and onlap) of depositional systems toward the distal eastern basin margin.

2008; Starck and Schulz, 2017). Farther north, at 22–23°S, these orange cross-bedded eolian sandstones become light gray due to diagenetic alteration of the Tranquitas Formation (Starck et al., 2018). This eolian interval is capped by fluvial deposits of regional extent, including the Valle Grande Formation in the west and the “Terciario Subandino” unit in the east (Hernández et al., 1996, 2005; Siks and Horton, 2011).

Farther south, multiple exposures across an E-W profile at ~26°S (Fig. 5) enable proximal to distal correlations of the progradational package across the basin (Fig. 6A). In the Calchaquí Valley (Site 4, 25.4°S), the progradational package encompasses the Angastaco Formation, which presents a lower sandy eolian Tintin Member and an upper sandy/gravelly fluvial/alluvial fan Las Flechas Member (del Papa et al., 2013a, 2013b). To the east, in the Lerma Valley (Site 3, 25.6°S), the eolian facies persist into the Río Seco Formation but the proximal fluvial/fan facies pass into ephemeral fluvial deposits of the Jesús María Formation. Farther eastward these units grade distally into playa or playa-lake deposits of the Anta Formation. The lateral continuity of the eolian units (Tintin Member of Angastaco Formation, Río Seco, San Lorenzo, and Tranquitas Formations) point to an extensive desert composed of dune fields and sand sheets, with limited development of muddy interdune areas.

The geographic distribution of the eolian units is well constrained, and was likely confined to the Miocene foredeep (Fig. 1 and 6A). In the north, eolian facies pinch out due to onlap and stratigraphic condensation against local basin margins near the Bolivian border (Starck et al., 2018). In more-proximal zones to the west, progressive thinning of eolian facies and a lateral change to fluvial and alluvial-fan facies is observed in the Cianzo, Angastaco and Pucará areas. In the south and southeast, eolian deposits are replaced by playa and playa-lake facies (Anta Formation and its southern equivalent, the San José Formation), a transition preserved in the Calchaquí Valley (near Cafayate) and Lerma Valley (near Alemania).

Geochronological data help define the depositional ages of the eolian sandstones and related units (Figs. 2 and 4). In the Calchaquí Valley, an early Miocene age is confirmed by a 21.0 ± 0.8 Ma zircon U-Pb age from an intercalated tuff in the Tintin area (del Papa et al., 2013a, 2013b). Similarly, a 22–19 Ma range for the youngest detrital zircon U-Pb ages is reported for sandstones in the Pucará and Angastaco areas (Carrapa et al., 2012; Galli et al., 2014). To the east, tuff horizons in the Tonco area yield slightly younger zircon U-Pb ages of 17.5 ± 0.1 Ma and 17.3 ± 0.2 Ma (Payrola et al., 2020). These ages are consistent with generally Oligocene ages for underlying deposits, including a maximum age of 28.7 ± 1.9 Ma (apatite fission track) reported for a cobble ~60 m below the eolian interval in the Monte Nieva area (DeCelles et al., 2011). Collectively, the available age constraints indicate a ca. 22 to 17 Ma age for major eolian deposition in these sectors (Sites 1–4) of the Eastern Cordillera, Santa Barbara system, and Subandean Zone.

West of this sand desert, a zone of comparable eolian facies has been described in the Puna Plateau (Sites 5–6). Eolian-bearing units include the Vizcachera Formation (lower member) in the Arizaro basin (Site 5; DeCelles et al., 2015; Vandervoort et al., 1995) and the Quiñoas (upper member) and Chacras Formation adjacent to the Salar de Antofalla (Kraemer et al., 1999; Voss, 2002). As in the east, eolian sandstones were progradationally overlain by fluvial/alluvial-fan facies followed by shaly and evaporitic facies. K-Ar and U-Pb results for several interbedded ashes define age spans of ca. 24–18 Ma and ca. 21–16 Ma for eolian sedimentation in the Antofalla and Arizaro localities, respectively (Kraemer et al., 1999; DeCelles et al., 2015).

3.2. West-central Argentina

The west-central basin segment (28–32°S) contains well-documented Miocene eolian facies within both the Precordillera (the frontal segment of the Andean fold-thrust belt) and the flanking Sierras Pampeanas region in the eastern foreland (Fig. 1). The eolian deposits persist along strike over a ~500 km N-S distance, across the Catamarca,

La Rioja and San Juan provinces of Argentina. However, thin- and thick-skinned shortening has structurally disrupted the original foreland basin, resulting in many separate Cenozoic outcrop belts (Fig. 2, Sites 7–18). Although discrete stratigraphic units were commonly defined and restricted to individual outcrop belts, age determinations from magnetostratigraphic, fission-track, $^{40}\text{Ar}/^{39}\text{Ar}$, and U-Pb geochronological methods have enabled chronostratigraphic correlations over large distances (e.g., Johnson et al., 1986; Reynolds et al., 1990; Jordan et al., 1990, 1993, 1996, 2001; Tabbutt, 1990; Dávila and Astini, 2007; Zambrano et al., 2011; Melchor et al., 2013; Vizán et al., 2013; Ciccioli et al., 2014a; Levina et al., 2014; Collo et al., 2017; Fosdick et al., 2017; Galli et al., 2017; Capaldi et al., 2020; Plonka et al., 2023).

The thickest and most complete successions are preserved in the north (Sites 7–12; Fig. 2), near 28–30°S at: (A) Fiambalá and Corral Quemado (Site 7, 27.7°S); (B) Sierra de Famatina (Site 8, 28.7°S); (C) Vinchina (Sierra de los Colorados) (Site 9, 28.7°S); Quebrada Santo Domingo area (Site 10, 28.5°S); (C) La Cueva (Site 11, 29.2°S), and (D) Las Juntas, including La Flecha and Troya localities (Site 12, 29.4°S) (Fig. 6B). Among these sites, the Vinchina region is distinguished by an exceptional, 0.5–1 km thick interval of stacked eolian sandstones within the lower Miocene Vallecito Formation (Tripaldi and Limarino, 2005; Tripaldi, 2012; Ciccioli et al., 2010, 2011), which is overlain by an upward coarsening 5–8 km thick package of fluvial and alluvial-fan facies of the middle Miocene Vinchina Formation (Jordan et al., 1993; Tripaldi et al., 2001; Limarino et al., 2001; Stevens Goddard et al., 2020).

In the south, a correlative lower Miocene eolian succession can be traced across multiple thrust sheets within the Precordillera segment of the fold-thrust belt (Sites 13–18). Along a broad swath at 30–32°S, including exposures near the city of San Juan, cross-bedded eolian sandstones have been assigned various stratigraphic names. The Vallecito Formation is identified in the Precordillera at 30–31°S, including: (A) Huaco (Site 13, 30.2°S); (B) Río Francia (Site 14, 30.6°S); and (C) Río Azul (Site 15, 30.7°S). Other eolian units identified in the Precordillera include the Cuculí Formation (lower member) in the Talacasto area (Site 16, 31.0°S), a well-exposed, up to 600 m thick eolianite that rests unconformably on Paleozoic strata (Milana, 1993; Levina et al., 2014; Bracco et al., 2015). Within the Río San Juan Valley, similar facies have been described for the Pachaco Formation (Site 17, 31.3°S; Cevallos and Milana, 1992; Milana et al., 1993).

The eolian deposits of west-central Argentina represent dune fields, sand sheets, or an integrated erg over an estimated >30,000 km² area. There are no definitive data demonstrating a physical connection between the eolian facies at 28–32°S with age-equivalent eolian deposits of the northwestern basin at 22–26°S. Thus, the original depositional zones may have been separated by a spatial gap of up to ~250 km where no eolian facies are preserved. This eolian gap contains Miocene fluvial and lacustrine facies that unconformably rest on Precambrian to lower Paleozoic igneous or metamorphic basement. West of the Precordillera, the Manantiales basin of the Frontal Cordillera contains eolian deposits of the “Areniscas Chocolate” within the lowermost Chinches Formation (Site 18, 32.0°S), which rests unconformably on Permian-Triassic igneous and sedimentary rocks (Jordan et al., 1996; Ramos, 1996; Pérez, 1995, 2001).

An early Miocene age for eolian deposition is confirmed by zircon U-Pb ages for sandstones and tuffaceous horizons, listed here from north to south. In the Fiambalá area (Site 7), detrital zircon U-Pb results provide maximum depositional ages (MDAs) of 23.9 ± 1.0 and 23 ± 1 Ma for eolian deposits, with MDAs of 16.2 ± 4.6 Ma and 15.4 ± 0.5 Ma for overlying fluvial deposits (Carrapa et al., 2008; Safipour et al., 2015; Deri et al., 2019, 2021). For the widespread Vallecito Formation (Sites 9–15), a broad range of possible ages is defined by MDAs of the underlying Puesto La Flecha Formation (ca. 38–32 Ma; Jordan et al., 1993; Fosdick et al., 2017) and the overlying Vinchina and Cerro Morado Formations (ca. 18–12 Ma; Limarino et al., 2002; Ciccioli et al., 2014a; Capaldi et al., 2020; Mackaman-Lofland et al., 2022). Direct ages from

the Vallecito Formation include MDAs of 19.4 ± 0.7 Ma and 18.6 ± 0.4 Ma in the Vinchina area (Site 9; Collo et al., 2011; Stevens Goddard and Carrapa, 2018) and 22.3 ± 1.6 Ma age near La Cueva-Las Juntas (Sites 11–12; Mackaman-Lofland et al., 2022). MDA results for lower to intermediate levels of the eolian succession in the Talacasto and Pachaco areas (Sites 16–17) range from 24.0 ± 1.2 Ma to 19.0 ± 0.6 Ma. Recognizing the potential for spatial variability, we tentatively infer an age range of 24–16 Ma for eolian deposition in the west-central basin segment, similar to Cicioli et al. (2023).

3.3. Cuyo and Neuquén basin segments

The Cuyo and Neuquén basin segments ($33\text{--}36^\circ\text{S}$) of the Mendoza province include eolian facies comparable to the northwestern ($22\text{--}26^\circ\text{S}$) and west-central ($28\text{--}32^\circ\text{S}$) segments of the Andean foreland basin in Argentina. However, in contrast to the more-northern zones, the Andean orogenic belt is considerably narrower in the south (Fig. 1). This contrast is mostly the product of the southward termination of the Precordillera, the ~ 100 km wide frontal segment of the fold-thrust belt at $28\text{--}33^\circ\text{S}$. Thus, in the south, the orogen is mostly defined by the Principal Cordillera and southern continuations of the Frontal Cordillera in the form of the Malargüe and Neuquén fold-thrust systems (Ramos et al., 1996, 2002; Giambiagi et al., 2012).

At $33\text{--}34^\circ\text{S}$, the Cuyo basin or Cacheuta basin, locally (Site 19, 33.1°S), contains a thick Neogene succession with eolian facies exposed in lower levels (Fig. 2) (Irigoyen et al., 2000; Buelow et al., 2018). In this region, near the city of Mendoza, eolian strata cap a fine-grained Paleogene interval of principally mudstones and associated pedogenic deposits. In turn, the eolian deposits are overlain by a progradational package of fluvial and alluvial-fan sandstones and conglomerates. The lower Miocene eolian deposits and middle Miocene fluvial deposits are included within a unified Mariño Formation. The eolian facies of the Mariño Formation are situated ~ 150 km from the nearest correlative eolian outcrops to the north (Site 17, Pachaco Formation), permissive of a potential gap in the early Miocene eolian sand dune fields and sand sheets (Fig. 1).

Depositional continuity of age-equivalent eolian facies has been confirmed in hydrocarbon wells throughout the Mendoza province south of 33°S . These subsurface deposits have been traced southward into eolian exposures of the northern continuation or Malargüe segment of the well-known Neuquén basin (Figs. 1 and 2). In the Sosneado region (Site 20, 35.1°S), the Agua de la Piedra Formation contains eolian sandstone facies equivalent to the lower Mariño eolianites (Site 19). Outcrops of the Agua de la Piedra eolian deposits can be traced as far north as $\sim 34.5^\circ\text{S}$, along the Diamante River at the foothills of the Frontal Cordillera. The lower Miocene record south of Malargüe has been mostly exhumed (Fuentes et al., 2016; Fuentes and Horton, 2020), so the southern depositional limit of the eolian facies is unknown.

Detrital zircon U-Pb ages for the eolian interval of the Mariño Formation in the Cuyo-Cacheuta area (Site 19) provide MDAs of 19.2 ± 0.3 Ma to 17.6 ± 0.3 Ma, with a 15.6 ± 1.0 Ma MDA for overlying non-eolian deposits of the upper Mariño Formation (Buelow et al., 2018). These ages are consistent with age constraints from magnetostratigraphic and $^{40}\text{Ar}/^{39}\text{Ar}$ results for the overlying middle to upper Miocene (ca. $16\text{--}8$ Ma) succession (Irigoyen et al., 2000). Correlative sandstones from the northern Neuquén basin (Malargüe fold-thrust belt) (including Sosneado, Site 20) yield similar U-Pb age constraints. The Agua de la Piedra Formation, which contains an eolian interval up to 200 m thick, exhibits MDAs ranging from 19.5 ± 0.4 Ma to 15.7 ± 0.6 Ma (Horton et al., 2016; Horton and Fuentes, 2016; Fuentes and Horton, 2020). An age range of ca. $20\text{--}16$ Ma is interpreted as the main phase of eolian conditions in this $33\text{--}36^\circ\text{S}$ segment of the foreland basin.

3.4. Basin chronostratigraphy

Existing chronostratigraphic data are consistent in identifying an

early Miocene age, and possibly latest Oligocene age, for eolian facies spanning the Andean foreland basin of central and northern Argentina (Figs. 1 and 2). The deposits occupy a remarkably similar stratigraphic position within the basin, at the base of a succession with a precursor fine-grained distal mudstone facies and an overlying very thick fluvial succession of sandstone and conglomerate (Figs. 3 and 4). These ages indicate a phase of deposition under arid conditions centered around $23\text{--}17$ Ma, with a maximum depositional duration from ca. 24 to 16 Ma, which approximately corresponds to the early Miocene sub-epoch.

Although some of the analyzed eolian intervals show shorter durations, this may reflect local variations in accommodation near proximal or distal basin margins during the early stages of regional desert conditions. This explanation seems appropriate for the distal eastern sectors of the basin, where a delayed onset of sediment accumulation can be inferred from the progressive onlapping relationship of eolian deposits onto pre-Mesozoic basement (Fig. 6). Alternatively, a shorter duration of eolian deposition may be the product of lateral facies variations, with replacement of eolian dunes by local fluvial or playa/playa lake systems developed under comparable arid conditions.

In addition to widespread early Miocene eolian deposition, restricted zones of older and younger eolian deposition have been identified locally. This includes eolian deposits of probable late Eocene-early Oligocene age in the Manantiales basin (Site 18; Pinto et al., 2018; Mackaman-Lofland et al., 2020; Suriano et al., 2023), and northern Bermejo basin (Sites 10–15; Fodick et al., 2015; Limarino et al., 2000, 2016; Reat and Fodick, 2018), and late Miocene age in the Vinchina-Quebrada Santo Domingo areas (Sites 9–10; Dávila and Astini, 2003, 2007; Amidon et al., 2016; Cicioli et al., 2005, 2014b; Marengo et al., 2019).

4. Sediment provenance

New and recently published detrital zircon U-Pb geochronological results, sandstone petrography, and paleocurrent measurements provide critical information on the provenance of the extensive eolian interval. Here we present background information on the U-Pb geochronological method, a regional summary of potential sediment source areas, and then a synthesis of new and published U-Pb ages and sandstone compositions for upper Oligocene-lower Miocene eolian deposits. The potential source areas include the magmatic arc to the west, the different segments of the fold-thrust belt, and uplifted basement blocks along basin margins in the foreland region. For eolian deposits, the provenance results implicate a series of local Andean sources and the magmatic arc, with little to no input from basement sources in the eastern foreland.

4.1. Detrital zircon U-Pb geochronology: methods

U-Pb geochronological analyses were conducted on detrital zircon grains from five samples. Following traditional physical and chemical mineral density separation techniques (including water table, heavy liquid and magnetic separation), a selection of inclusion-free zircon grains of variable size and shape were randomly selected and analyzed for U-Pb geochronology on the Element2 LA-ICPMS (laser-ablation inductively coupled plasma mass spectrometer). Samples ADP225, ADP224, and SSN224 were analyzed as polished mounts at the University of Arizona LaserChronCenter (Gehrels et al., 2008). Samples AZL01 and AZL02 were analyzed as grain mounts at the University of Texas (Capaldi et al., 2020). We report new U-Pb geochronological results with measured age uncertainties of $1\text{--}2\%$ (1σ error). We use $^{206}\text{Pb}/^{238}\text{U}$ ages for zircons younger than 1200 Ma and $^{206}\text{Pb}/^{207}\text{Pb}$ ages for zircons older than 1200 Ma. Individual analyses were filtered such that results displaying $>20\%$ discordance or $>5\%$ reverse discordance were excluded from further consideration. Results for individual samples are represented as kernel density estimations (KDEs) with a bandwidth of 15 Myr and histogram age bins with 25 Myr bin widths. Detrital

zircon U-Pb geochronological data are reported for all samples (Supplemental File S1).

4.2. Potential sediment sources

The dominant sediment source regions for the Oligocene-Miocene

eolian systems of the southern central Andean foreland include the Andean magmatic arc and incipient retroarc fold-thrust belt to the west and South American cratonic rocks that comprise the Sierras Pampeanas to the east (Fig. 7). These source regions yield distinctive detrital zircon geochronology age distributions and sandstone composition provenance signatures that can be readily distinguished from one another.

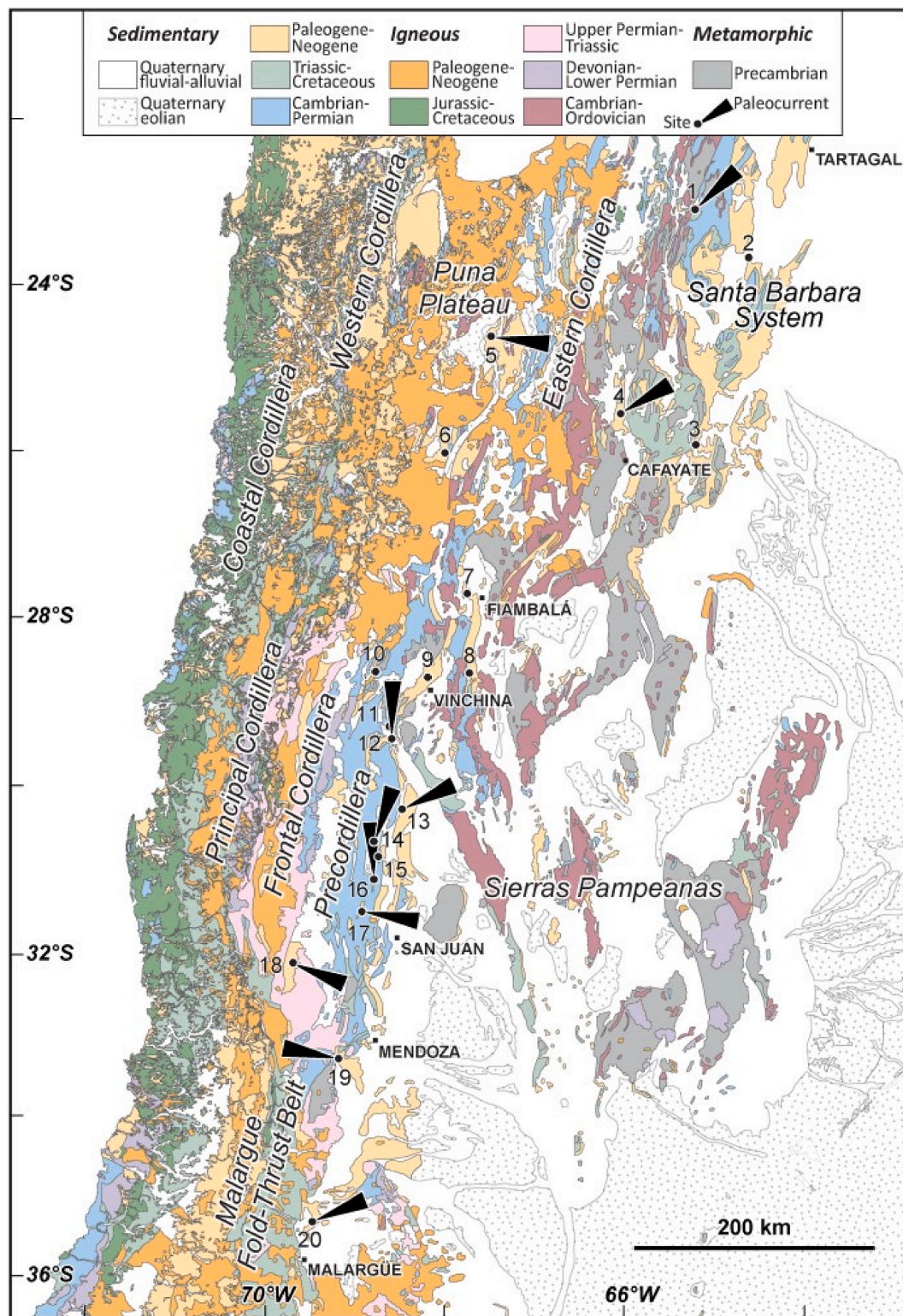


Fig. 7. Geologic map of the southern central Andes highlighting major sediment sources (from Servicio Geológico Minero SEGEMAR, 1999; 2012; Sernageomin, 2003), and paleocurrent measurements (black triangles) at Site locations (numbered black circles).

Here we describe diagnostic age groups representative of sediment provenance signatures recorded by detrital zircon U-Pb analyses from basement terranes (440–1450 Ma), Gondwanan magmatism (380–200 Ma), and Andean arc magmatism (200–0 Ma). Proterozoic aged zircons (~925–1450 Ma) may have been sourced from numerous Sunsás metamorphic basement units that presently crop out across the Sierras Pampeanas and Arequipa-Antofalla basement blocks, and is ubiquitous in most Ordovician to Permian sedimentary sequences deformed within the Andean fold-thrust belt (Ramos, 2004; Rapela et al., 2016). The Eastern Sierras Pampeanas (550–725 Ma) age group is initially sourced from metasedimentary rocks (e.g., Puncoviscana Formation) and commonly recycled from Carboniferous to Permian strata in the Andean fold-thrust belt (Fosdick et al., 2015; Capaldi et al., 2017, 2020) and Cambrian-Ordovician strata of the Eastern Cordillera (Calle et al., 2023). Cambrian to Ordovician ages (550–440 Ma) are derived from igneous rocks throughout the western Sierras Pampeanas and Puna plateau (Fig. 7). This group involves the dominant 515–550 Ma age peak originally from igneous-metamorphic rocks of the Pampean magmatic arc presently exposed in the Sierras de Córdoba (Rapela et al., 2016) and 440–505 Ma Famatinian continental arc rocks (Otamendi et al., 2017; Rapela et al., 2018) and subsequent 385–435 Ma metamorphic assemblages associated with accretion of the Cuyania terrane (Coira et al., 1982; Astini et al., 1995). Recycled Famatinian and Pampean age components are derived from Silurian-Devonian and Carboniferous-Permian sedimentary units in the Precordillera fold-thrust belt (Capaldi et al., 2017) and are ubiquitous in the Cambrian-Ordovician strata of the Eastern Cordillera (Calle et al., 2023).

Late Devonian to Early Carboniferous (380–320 Ma) magmatism was expressed as widely distributed (>500 km) granitic plutons emplaced during extensional conditions (Dahlquist et al., 2018; Moreno et al., 2020). Carboniferous-Triassic zircon ages are derived from intrusive and volcanic rock sources throughout the Chilean Coastal Cordillera, Frontal Cordillera, and Principal Cordillera (Fig. 7). These rocks include the 290–310 Ma Elqui-Limari and Colanguil batholiths (Hervé et al., 2014; del Rey et al., 2016), 240–285 Ma granitoids and silicic volcanic rocks of the Choiyoi igneous province (Mpodozis and Kay, 1992; Kleiman and Japas, 2009; Sato et al., 2015), and 240–200 Ma Upper Triassic volcanic and volcanioclastic rocks (Oliveros et al., 2018). Additional sources of Permian-Triassic age components include recycled Jurassic to Cretaceous sedimentary deposits in the Principal Cordillera (Mackaman-Lofland et al., 2019) and Triassic strata from the Eastern Cordillera (Calle et al., 2018).

East-dipping subduction generated the Jurassic to Cenozoic Andean magmatic arc (200–0 Ma), which is defined by north-trending belts involving principally granite/granodiorite intrusions and andesite volcanic rocks. These belts young systematically eastward from Jurassic (190–140 Ma) and Cretaceous (125–65 Ma) rocks along the Chilean coast, to Paleocene–Eocene (65–35 Ma) and Eocene–Oligocene (35–25 Ma) units along the western flank of the Principal Cordillera, and finally Miocene (25–5 Ma) volcanic rocks in the eastern Principal Cordillera, Frontal Cordillera, and Argentine foreland (Kay et al., 1991; Haschke et al., 2006; Jones et al., 2016; Balgord, 2017; Capaldi et al., 2021). Primary sources of the Andean arc age components are likely derived from erosional unroofing of Jurassic to Paleogene intra-arc and retroarc basin deposits (Fig. 7; Capaldi et al., 2017; Garzanti et al., 2022).

Petrography of modern river and Holocene eolian dune sand can be leveraged to identify provenance signatures of the Andean arc, fold-thrust belt, and craton sources in the retroarc of Argentina between 28 and 36°S (Tripaldi et al., 2010; Garzanti et al., 2021, 2022). Eolian sands derived from cratonic basement assemblages are predominately composed of ~50% quartz and ~40% feldspar (plagioclase) with ~10% lithic fragments. Whereas eolian sands derived from the Andean arc and fold-thrust belt exhibit a progressive southward increase in lithic fragments (volcanic > sedimentary > metamorphic) components and corresponding decrease in quartz (Garzanti et al., 2022).

4.3. Detrital zircon U-Pb geochronology: results

Vallecito Formation samples AZL01 and AZL02 from the Rio Azul area (Site 15) show similar age distributions that are dominated by a late Oligocene to early Miocene (20–32 Ma) age peak (Fig. 8). Rio Azul samples record a minor age peak spanning Permian-Triassic (200–280 Ma) and Devonian-Permian (280–380 Ma) age groups. Agua de la Piedra Formation samples collected from Sosneado (Site 20) in the Malargüe region display multi-modal age distributions that include: a scattered distribution of young Andean arc ages with a minor amount of Oligocene-Miocene ages and Cretaceous-Paleocene ages; a strong Jurassic age peak around 170 to 200 Ma; significant amount of ages within the Permian-Triassic (200–280 Ma) and Devonian-Permian (280–380 Ma) age groups with a peak around 255–270 Ma; and a diffuse tail of Cambrian-Ordovician (440–550 Ma), Eastern Sierras Pampeanas (550–725 Ma), and Sunsás (925–1450 Ma) ages. Collectively, the eolian sandstones samples exhibit similar detrital zircon age distributions amongst sampled collected from each depocenter (Fig. 8 and S1), allowing us to group individual samples into composite age distributions based on depocenter regions.

4.4. Provenance of eolian sandstones

Detrital zircon U-Pb age populations and paleocurrent measurements reveal sediment provenance variations in eolian deposition and provide insight into late Oligocene-Miocene erosion and along-strike evolution of different segments of the Andean foreland basin. Paleocurrent measurements from 10 Sites (Fig. 7) record major westerly winds, transporting Andean detritus broadly eastward to the foreland basin with common axial northward deflections (Cevallos and Milana, 1992; Tripaldi and Limarino, 2005; Siks and Horton, 2011; Galli et al., 2014; DeCelles et al., 2015; Horton et al., 2016; Fosdick et al., 2017; Buelow et al., 2018; Capaldi et al., 2020; Mackaman-Lofland et al., 2020).

New and previously published data from the following eolian-bearing rock units across 11 sites are compiled and plotted as U-Pb age distributions (Fig. 9): Casa Grande Formation in the Cianzo area (Site 1; Siks and Horton, 2011); Angastaco Formation in the Calchaquí section (Site 4; Carrapa et al., 2012; Galli et al., 2014); Vizcachera Formation in the Arizaro basin (Site 5; DeCelles et al., 2015); Vallecito Formation at the Las Juntas locality (Site 12; Mackaman-Lofland et al., 2022), Huaco and Rio Francia (Sites 13–14; Fosdick et al., 2017), Rio Azul (Site 15; this study), and Talacasto areas (Site 16); the Pachaco Formation in the Pachaco section (Site 17; Levina et al., 2014); Marín Formation in the Cuyo (Cacheuta) basin (Site 19; Buelow et al., 2018); and Agua de la Piedra Formation in the Sosneado area of the Malargüe basin (Site 20; Horton et al., 2016; this study). Further information on these eolian sandstone samples is provided in Supplemental File S2 and individual KDEs are plotted in Supplemental File S3.

Detrital zircon age distributions for eolian sandstones from the northwestern basin (Cianzo, Arizaro, and Calchaquí sites) display pronounced Cambrian-Ordovician (440–550 Ma), Eastern Sierras Pampeanas (550–750 Ma), and Sunsás (925–1450 Ma) ages (Fig. 9). These Precambrian to earliest Paleozoic age components are commonly not present in basin segments to the south (28–36°S). These older zircons were largely sourced from Cambrian to Ordovician stratigraphic units found throughout the Eastern Cordillera (Calle et al., 2023). The presence of eroded material from the Eastern Cordillera in the northern retroarc basin is consistent with structural reconstructions for the broad segment of the central Andes that document a late Oligocene (~28–24 Ma) phase of increased shortening and thrust front propagation (Carrapa and DeCelles, 2015; Anderson et al., 2017, 2018).

The zircon U-Pb age distributions for the eolian Vallecito and Pachaco Formations in the west-central basin include a significant amount of Permian-Triassic (200–280 Ma) and Devonian-Permian (280–380 Ma) ages (Fig. 9). These pre-Cenozoic ages indicate erosion of pre-Andean intrusive and extrusive igneous rocks in addition to

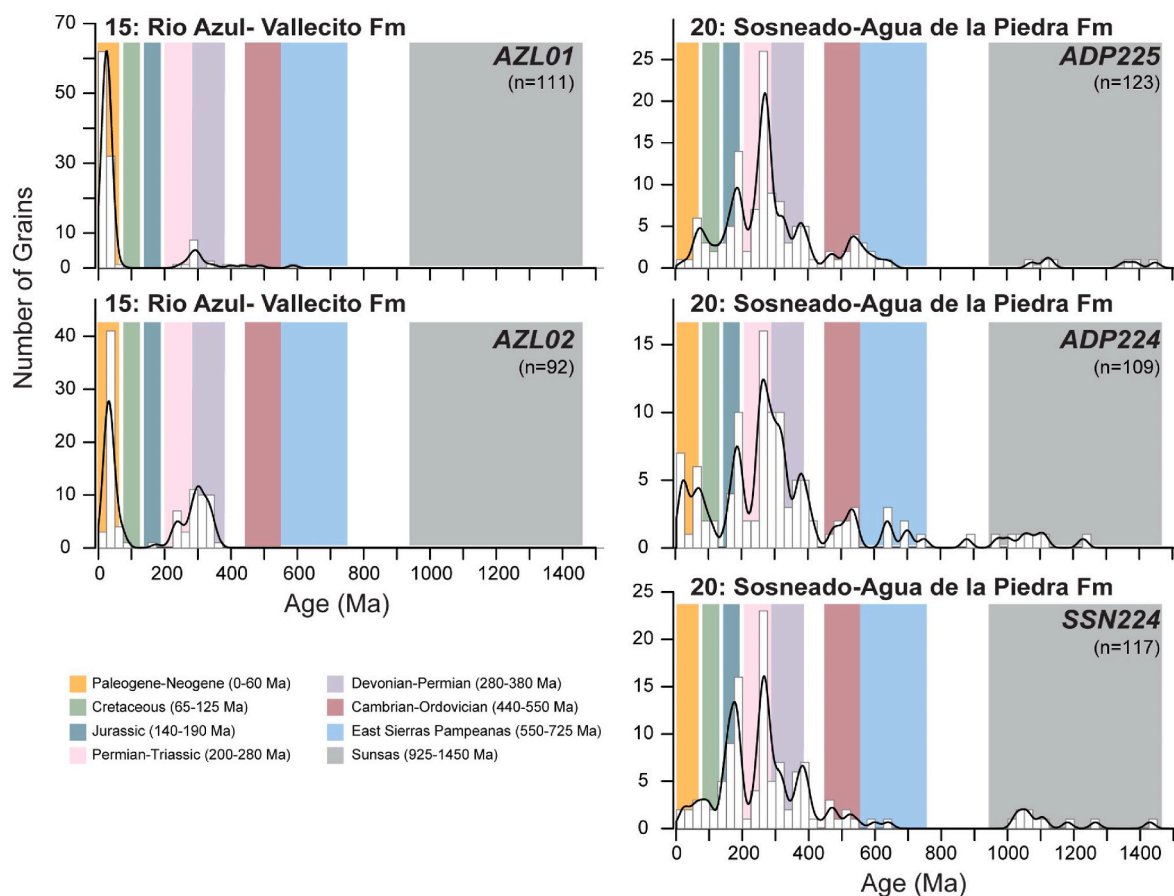


Fig. 8. Comparative plot of detrital zircon U-Pb age distributions for new sandstone samples from the Rio Azul (Site 15) and Malargüe-Sosneado (Site 20) localities. Age distributions are depicted as kernel density estimates (KDEs, with 15 Myr bandwidth) and age histograms (25 Myr bin width) with emphasis on key age components (color shading).

recycling of Jurassic to Paleogene basin deposits across the Principal Cordillera. Apatite fission track dates from the Principal Cordillera at 28–32°S reveal earliest Miocene exhumational cooling of the Principal Cordillera (Rodríguez et al., 2018) that coincides with initial retroarc foreland basin development (Jordan et al., 1993; Levina et al., 2014; Capaldi et al., 2020).

Farther south, the Mariño Formation in the Cuyo depocenter displays age distributions similar to the Vallecito Formation with a prominent Permian-Triassic age component, but also contains a minor Mesozoic age component and spread of older (>400 Ma) ages. The Agua de la Piedra Formation from the Malargüe depocenter exhibits a unique detrital zircon age distribution with Cretaceous and Jurassic ages in addition to a prominent Permian-Triassic age peak. In the southern basin segment, eolian sediment was derived from Mesozoic strata incorporated into the Malargüe fold-thrust belt during the early Miocene (Horton et al., 2016; Fuentes et al., 2016).

Along-strike comparisons of paleocurrents and detrital zircon age signatures highlight several trends during widespread eolian deposition. First, the consistent influence of the Andean magmatic arc as a regional source of sediment is indicated by ubiquitous Mesozoic-Cenozoic ages and northeast-directed eolian paleocurrents. Second, minimal direct input from eastern cratonic regions is suggested by the diminished proportion of Precambrian age signatures. Third, and most significantly, the presence of several distinct age populations restricted to particular segments of the foreland basin reveals a spatial segregation of local sediment sources along strike within the Andean fold-thrust belt.

The along-strike variations in eolian sediment sources detected by detrital zircon geochronological data are supported by previously reported sandstone petrographic results (Fig. 10). Sandstone data from the

northwestern basin segment (Sites 1–5; 22–26°S) include the Casa Grande, Angastaco, and Rio Seco Formations, which consist of high proportions of polycrystalline quartz and metamorphic lithic fragments indicative of Eastern Cordillera metasedimentary sources (Siks and Horton, 2011; Galli et al., 2014, 2023). The Vizcachera Formation (Arizaro basin) has similar compositions as the regionally extensive Vallecito Formation of the central-western basin segment (Sites 6–18; 28–32°S), where all samples exhibit greater amounts of feldspar and volcanic lithic fragments, with correspondingly less quartz than than the northwestern basin segment (DeCelles et al., 2015; Fosdick et al., 2017; Reat and Fosdick, 2018; Tamagno et al., 2018). The increased volcanic component likely reflects erosion of the magmatic arc province of the Principal Cordillera. In the southern basin segment (Sites 19–20), sandstones from the Mariño and Agua de la Piedra Formations from the Cuyo (Cacheuta) and Malargüe (northern Neuquén) areas exhibit severely reduced quartz content and the highest amount of volcanic lithic fragments (Arcila Galledo, 2010; Buelow et al., 2018). This immature sediment was derived principally from the adjacent magmatic arc and associated strata incorporated into the narrow fold-thrust belt at 33–36°S.

At a regional scale, the sandstone petrographic results show a tremendous along-strike variation in provenance that can be related to the position of the magmatic arc, the width of the fold-thrust belt, and the timing of earliest thrust-belt development. We suggest that the spatial proximity to the magmatic arc explains the compositional immaturity and high proportions of volcanic lithic fragments, at the expense of quartz, in more southern areas with a narrow fold-thrust belt. In northern areas, the combination of earlier (Eocene-Oligocene) shortening, a much wider fold-thrust belt spanning the Puna plateau and

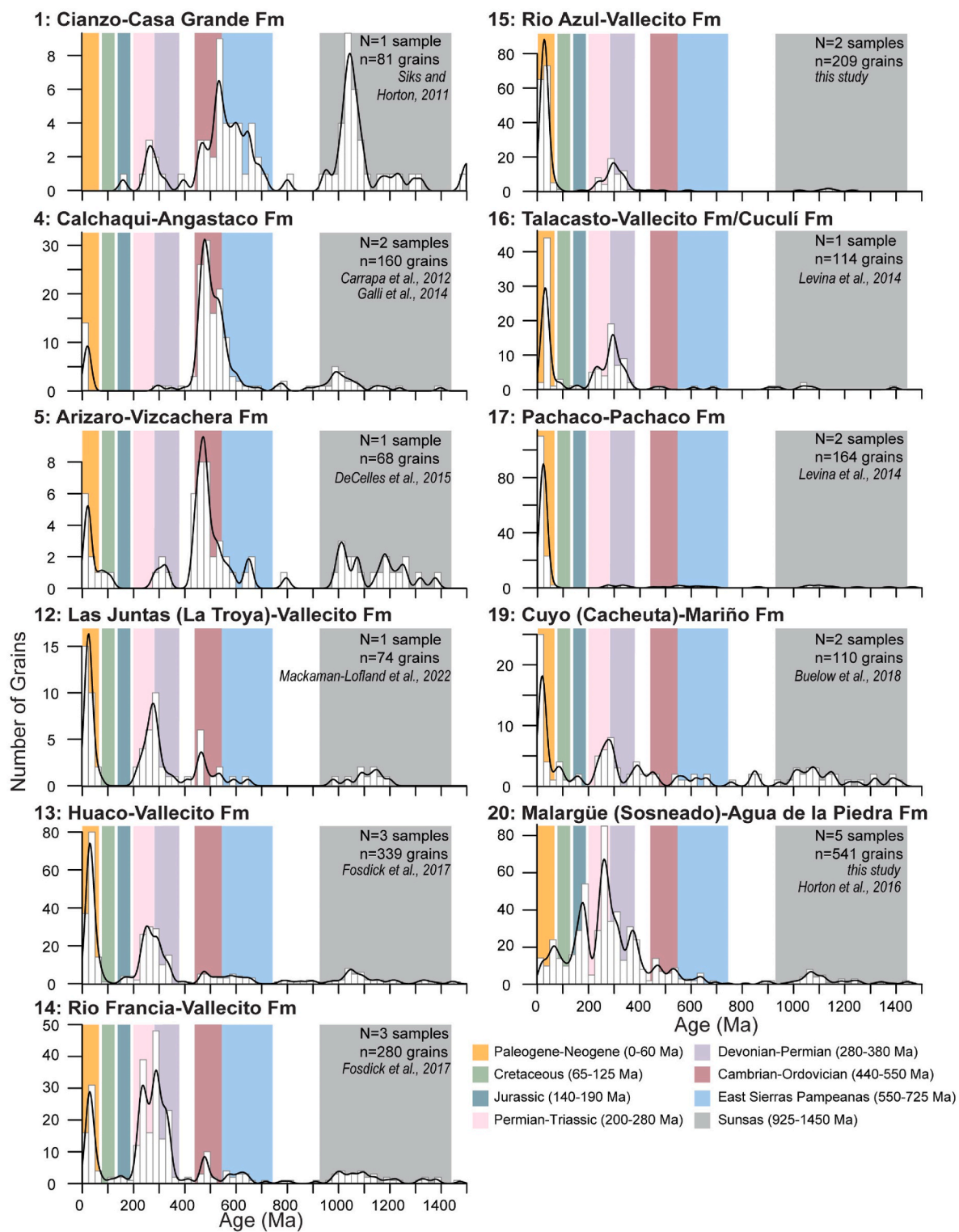


Fig. 9. Comparative plot of detrital zircon U-Pb age distributions for Oligocene-Miocene eolian sandstones from northwestern (Sites 1–5), west-central (Sites 6–18), and southern (Sites 19–20) basin segments. Age distributions are depicted as kernel density estimates (KDEs, with 15 Myr bandwidth) and age histograms (25 Myr bin width) with emphasis on key age components (color shading).

Eastern Cordillera, and a greater distance from active magmatic sources collectively promoted deposition of more mature sandstones with high proportions of quartz relative to feldspar and lithic fragments.

5. Sediment accumulation history and tectonic significance of eolian deposits

Integration of sediment accumulation records from 8 sites within the Andean foreland basin (Fig. 11) indicates a strikingly similar subsidence history for the lower Miocene eolian interval. For each locality, a single

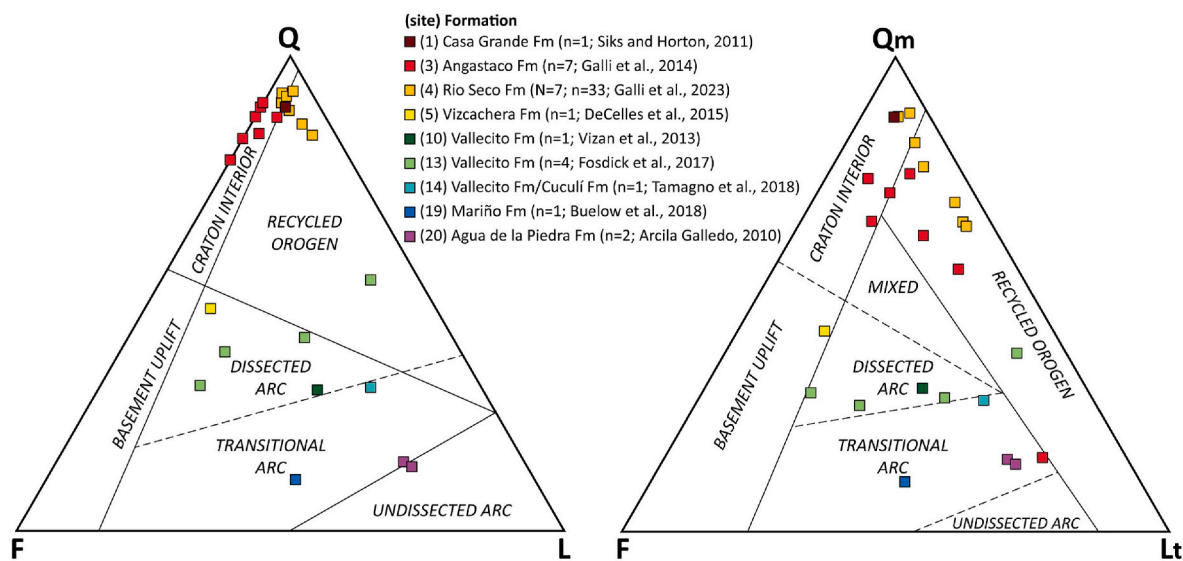


Fig. 10. Sandstone modal petrographic data from Oligocene-Miocene eolian deposits. Tectonic provenance fields from Dickinson, 1985: Q-quartz, Qm-monocrystalline quartz, F-feldspar, L-lithic fragments, Lt-total lithic fragments (including chert).

sediment accumulation curve shows stratigraphic thickness (or depth) over time. Each curve represents new and available information on stratigraphic thickness (undecompressed) and depositional age (Johnson et al., 1986; Reynolds et al., 1990; Starck, 2011; Horton and Fuentes, 2016; Buelow et al., 2018; Fuentes and Horton, 2020; Capaldi et al., 2020; Mackaman-Lofland et al., 2022).

Comparison of the sediment accumulation history with the timing of eolian deposition indicates a distinct and recurring theme in the tectonic evolution of the basin. Specifically, the eolian facies are consistently located at, or very near, the base of the main foreland basin succession (Figs. 2–6). As discussed above, eolian conditions persisted for several millions of years, with a maximum duration from ~24 to ~16 Ma. In the sediment accumulation plots, this phase of eolian deposition coincided with the roughly 23–18 Ma onset of rapid sediment accumulation across proximal (western) sectors of the studied retroarc region. More specifically, the eolian facies are located in the convex-upward part of the sediment accumulation curve that defines the narrow transition from an early period of slow accumulation or non-deposition (Horton and Fuentes, 2016; Fuentes and Horton, 2020) to the main phase of rapid flexural subsidence (Jordan et al., 2001). This situation can be traced within the western basin exposures for ~1500 km along strike, parallel to the north-trending Andean orogenic belt, suggestive of a correlation between regional climatic and tectonic conditions.

The preferential occurrence of eolian facies during the early phase of rapid subsidence could be construed as an indicator of a sediment-starved or underfilled basin situation, wherein subsidence and accommodation surpass sediment accumulation. This interpretation may further suggest that the arid conditions necessary for eolian deposition also prevented sufficient sediment supply to the high-accommodation basin, such that alluvial-fan and fluvial deposits were restricted to the proximal basin margin adjacent to the orogenic front. The lack of throughgoing rivers for the vast majority of the basin meant that sediment input from waterlain processes was replaced by eolian deposition, with a net accumulation rate lower than the available accommodation. If this starved basin model is correct, then the sediment accumulation plots (Fig. 11) represent the minimum amount of subsidence rather than the total value of accommodation generated.

6. Discussion

Stratigraphic, provenance, and sediment accumulation histories reveal a huge desert with pervasive eolian conditions in northern and

central Argentina during latest Oligocene through early Miocene time. The Andean retroarc region from 22° to 36°S (Fig. 1) was characterized by eolian sand dunes and sand sheets with intermittent ephemeral fluvial systems in interdune settings. Regional chronostratigraphic correlations indicate a principally ~24 to 16 Ma age range for eolian conditions (Figs. 2–4), contemporaneous with the regional establishment of an integrated foreland basin system during pronounced shortening and growth of the retroarc fold-thrust belt.

Long-lived eolian conditions in foreland basins are uncommon and likely require a combination of specific factors in terms of aridity (low precipitation), atmospheric circulation, orography, sediment dispersal, and sediment accommodation space. Here we consider the climatic and tectonic context for eolian processes in the southern central Andes and adjacent foreland (over a ~1500 km N–S distance and likely >100,000 km² depositional area), with implications for Andean paleogeography, sediment source areas, prevailing winds, and regional subsidence patterns.

The sustained aridity over this large region can be evaluated in the context of two perspectives. First, arid conditions may be the product of global or regional climate variations mostly independent of Andean tectonic processes. In this case, aridification would be unrelated to any shifts in deformation and exhumation of sediment source areas within the Andes. Alternatively, aridification may reflect rain-shadow development and changes in atmospheric circulation governed by rapid topographic growth during the main phase of shortening and deformation advance in the Andean orogenic belt.

6.1. Regional climatic processes

The southern central Andes have remained at similar latitudes over the past 20–30 Myr, on the basis of plate reconstructions showing a nearly due westward motion of the South American plate (Maloney et al., 2013; Horton, 2018a). The retroarc study region at 22–36°S is situated within the broad transitional zone between easterly trade winds at low latitudes (generally 0–30°S) and westerly winds at mid latitudes (generally 30–60°S). The precise boundary between these two zones is subject to variations in the size and configuration of the continent and adjacent ocean basins, as well as topographic variations within the continent (e.g., Horton, 1999; Montgomery et al., 2001; Strecker et al., 2007; Viale et al., 2019).

Global climate change near the Oligocene-Miocene boundary provides a potential mechanism for the abrupt appearance of desert

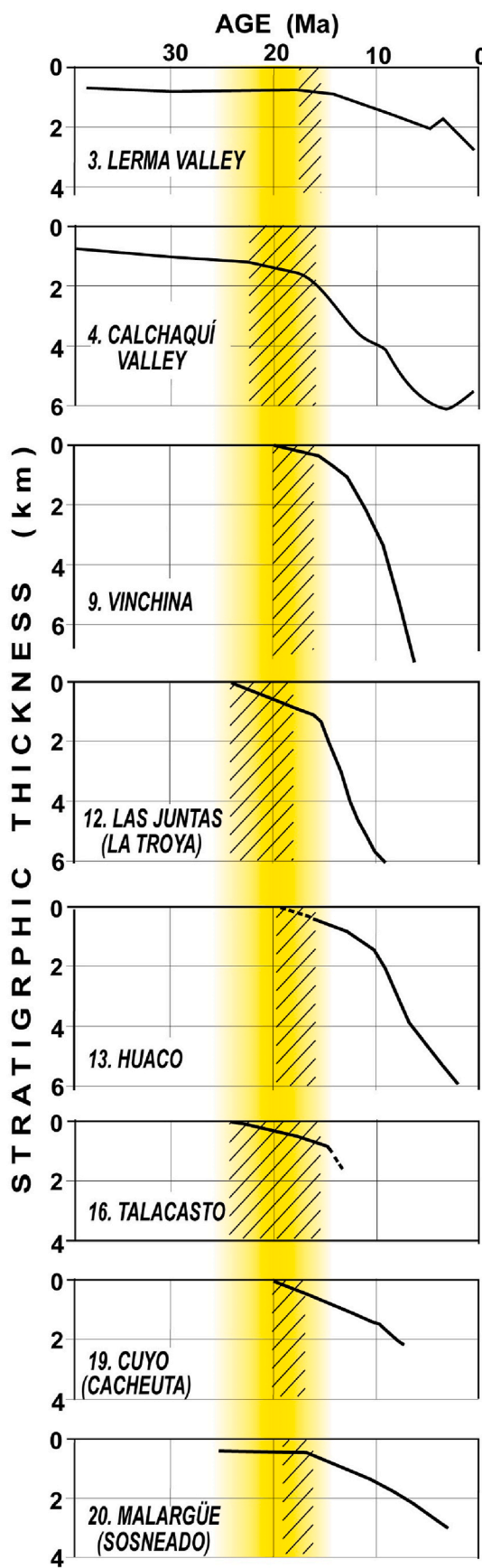


Fig. 11. Sediment accumulation plots for Cenozoic basin sites (Figs. 1 and 2) in the retroarc foreland basin of northern Argentina. The ruled pattern indicates the eolian interval in each locality. In yellow, the estimated time span for the regional eolian event. Source of the basin history curves for each site: 3: Starck, 2011; 4: this work; 9, 12 and 13: Mackaman-Lofland et al., 2022; 16: Levina et al., 2014; Capaldi et al., 2020; 19: Buelow et al., 2018; 20: Fuentes and Horton, 2020.

conditions in the study region. Although the Oligocene is widely regarded as a period of global cooling in relationship to the opening of Drake Passage and the growth of a significant Antarctic ice sheet, climate records for latest Oligocene to early Miocene time show considerable variability (Zachos et al., 1997; Pfuhl and McCave, 2005; Liebrand et al., 2017). In South America, it is possible that such variations, potentially linked to atmospheric CO₂, orbital forcing, or ice-climate feedbacks may have triggered increases in surface temperature that promoted aridification and protracted early Miocene eolian deposition in the retroarc region of northern and central Argentina.

A subsequent shift in regional climate during the Middle Miocene Climatic Optimum (MMCO) may have promoted global warming that was potentially manifest in continental regions by enhanced seasonality and the establishment or intensification of monsoon conditions (Steinthorsdottir et al., 2021). In the southern central Andes, such conditions would have inhibited eolian processes within this segment of the adjacent Andean foreland basin, consistent with the approximate termination of widespread eolian conditions at ~17–16 Ma (Fig. 2).

Similar mechanisms may be envisioned for isolated eolian deposits within older and younger basin fill, potentially linked to global climatic episodes. However, the emphasis of this study is the more-extensive regional desert conditions that commenced near the Oligocene-Miocene boundary. We infer that global or regional climate change may have impacted the study area through a reduction in precipitation and modification of prevailing winds, but would have had little to no impact on Andean topography, the location and composition of sediment source regions, or the magnitude of accommodation space within the foreland basin.

6.2. Regional tectonic processes

A combination of complementary tectonic processes in the southern central Andes may be responsible for sustained desert conditions that led to eolian deposition across large swaths of the retroarc foreland. First and foremost, rapid topographic growth during a documented period of enhanced shortening may have triggered the development of a rain shadow across the foreland basin. Although paleoelevation constraints are limited, we speculate that the growing topography exceeded the threshold conditions required to change regional atmospheric circulation. These thresholds likely include a combination of maximum and mean elevation of the orogenic belt, internal relief, and the width or breadth of high topography. An increased height and width of the Andean orogen would be expected as direct consequences of the enhanced rates and magnitudes of shortening and topographic advance in the early Miocene (e.g., Jordan et al., 1993, 2001; DeCelles et al., 2015; Giambiagi et al., 2022; Horton et al., 2022a; Mackaman-Lofland et al., 2022).

Second, increased shortening and deformation propagation into eastern retroarc regions would have provided fresh exposure of sedimentary and igneous rocks within the growing orogen in close proximity to the foreland basin. Prior to the early Miocene, many detrital provenance datasets point to the Andean magmatic arc as a dominant source of sediment (Arcila Gallego, 2010; Horton et al., 2016; Fosdick et al., 2017; Buelow et al., 2018; Horton, 2018b; Reat and Fosdick, 2018; Tamagno et al., 2018). In contrast, younger basin fill shows the appearance and volumetric dominance of materials eroded from the fold-thrust belt, primarily composed of pre-Andean igneous and sedimentary rocks (Jordan et al., 1993, 1996; Pérez, 2001; Ciccioli et al.,

2014b; Siks and Horton, 2011; Galli et al., 2014; Levina et al., 2014; DeCelles et al., 2015; Capaldi et al., 2020; Mackaman-Lofland et al., 2019, 2020; Suriano et al., 2017; Plonka et al., 2023).

Third, the requisite tectonic loading that accompanied increased shortening and crustal thickening in the early Miocene would have driven rapid generation of accommodation space in the foreland basin (e.g., Jordan et al., 1993, 2001; Capaldi et al., 2020; Mackaman-Lofland et al., 2022). Among other effects, this enhanced subsidence would have promoted preservation rather than redistribution of eolian sediments. Further, the eolian deposits recorded in the foreland stratigraphic record should be considered as a volumetric minimum in an underfilled basin, as it is likely that additional accommodation space existed but was not filled with sediment.

6.3. Reconstruction of tectonics, subsidence, and paleogeography

The latest Oligocene-early Miocene marks the inception of the main phase of Andean shortening and pronounced eastward advance of the fold-thrust belt. By inference, the initial construction of high topography in the orogenic belt at these latitudes induced aridification in a rain shadow that encompassed the retroarc foreland basin to the east. We present a three-step reconstruction (Fig. 12) that accounts for the latest Oligocene-early Miocene phase of eolian deposition and the preceding and ensuing development of the foreland basin.

Sediment accumulation records from 8 localities (Fig. 11) provide a sound basis for a synthesis of the sediment accumulation history of the retroarc foreland (Fig. 12A). This history involves three discrete phases of subsidence. Phase 1 involves severely limited retroarc subsidence with accumulation of a very thin stratigraphic section represented principally by Paleocene to lower Oligocene clastic deposits (Horton and

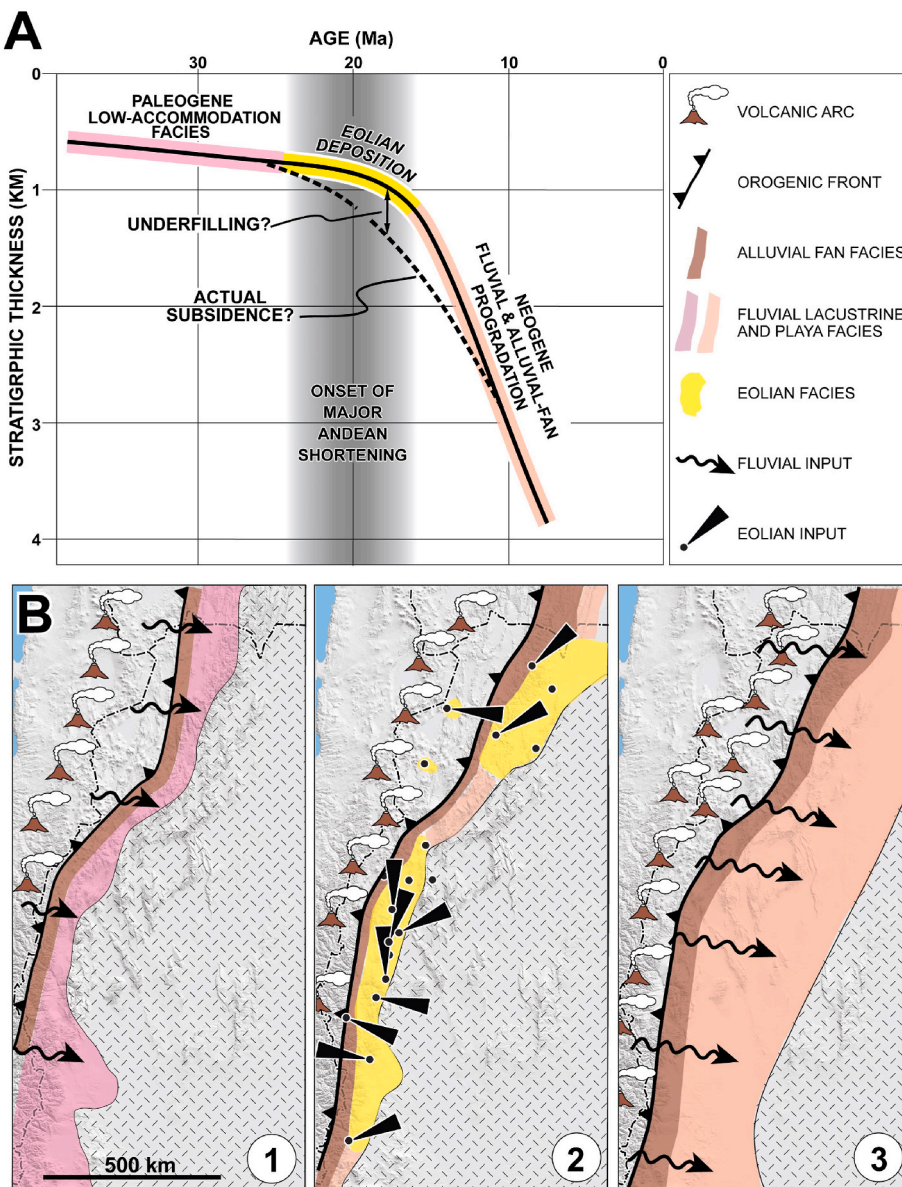


Fig. 12. (A) Schematic sediment accumulation plot and (B) paleogeographic maps depicting the three major stages in the middle to late Cenozoic evolution of the retroarc foreland basin of northern Argentina: (1) Paleogene accumulation of distal (fine-grained) retroarc facies during slow subsidence (shallow curve, red/purple); (2) deposition of eolian sandstone facies during latest Oligocene-early Miocene acceleration of subsidence (broad inflection in curve, yellow) with sediments transported by north-northeast wind s (Fig. 7); and (3) middle to late Miocene deposition and eastward progradation of thick alluvial fan to fluvial deposits during rapid subsidence (steep curve, brown). The depositional facies (and colors) correspond to time-stratigraphic basin transects (Fig. 6).

Fuentes, 2016; Horton, 2018a, 2018b). Phase 2 represents the inception of enhanced flexural accommodation, as represented by a several-fold increase in accumulation rates in the latest Oligocene to early Miocene. Phase 3 is defined by continued rapid accumulation of a thick middle Miocene to Quaternary succession.

The three phases are also characterized by contrasting depositional facies. Slow accommodation during Phase 1 was marked by accumulation of distal (fine-grained) facies in overbank fluvial and pedogenic environments with local lacustrine conditions. Phase 2 involved widespread deposition of eolian sandstone facies, both in proximal and distal sectors of the basin. Phase 3 recorded deposition and eastward progradation of thick alluvial fan to fluvial deposits during rapid subsidence.

Schematic paleogeographic maps show major components of the aforementioned three-step history (Fig. 12B, Phases 1–3). Emphasis is placed on the position and eastward advance of the Cenozoic magmatic arc, retroarc fold-thrust belt, and adjacent foreland basin. Within the foreland basin, the paleogeographic reconstructions highlight changes in depositional systems, sediment dispersal directions, and the overall position and width of the basin relative to the growing Andean orogenic belt.

- (1) Paleogene (Fig. 12B, Phase 1). A low-accommodation retroarc basin was fed sediment principally from the Andean magmatic arc. A narrow fold-thrust belt is inferred, but was likely subjected to a range of tectonic regimes, including neutral-stress conditions or low-magnitude extension, strike-slip, or shortening conditions. Flexural subsidence, albeit limited, was likely related to topographic loading by the magmatic arc and small-scale fold-thrust structures. Deposition involved distal fluvial, fluvial overbank, pedogenic, and limited lacustrine deposition.
- (2) Latest Oligocene-early Miocene (Fig. 12B, Phase 2). The inception of large-magnitude shortening, as defined by the growth and eastward advance of the fold-thrust belt, was accompanied by eastward advance of arc magmatism and the initiation of rapid flexural subsidence in the foreland basin. This phase is marked by widespread eolian conditions in the form of large sand dunes or an erg system. Aridification linked to topographic growth may have promoted eolian deposition within a sediment-starved or underfilled foreland basin with a high ratio of accommodation to sediment supply.
- (3) Middle Miocene–Quaternary (Fig. 12B, Phase 3). Continued rapid flexural subsidence in the retroarc foreland was driven by further shortening and topographic loading within the migrating fold-thrust belt. Facies changes indicate pronounced progradation of fluvial, fluvial megafan, and alluvial fan depositional systems. The cessation of widespread eolian conditions may have coincided with a shift in climate conditions (namely the onset of the Middle Miocene Climatic Optimum) and a drastically increased supply of synorogenic sediment that exceeded the rapid generation of accommodation space and resulted in regional progradation of coarse-grained clastic facies belts.

7. Conclusions

A widespread eolian depositional system defined the initiation of major subsidence in the Andean retroarc foreland during the main phase of Andean orogenesis in the southern central Andes. Systems of eolian dunes, sand sheets, and ergs are rare in foreland basins, suggesting a combination of favorable conditions during latest Oligocene to early Miocene sedimentation in the foreland basin of Argentina at 22–36°S. These conditions were related to: (1) climate—with foreland aridification and widespread desert conditions; (2) paleogeographic context—in terms of latitudinal controls and topographic highs that guide prevailing

winds and generate possible rain shadows; and (3) tectonic processes—in the form of crustal loading and the generation of accommodation space. New and previously published paleocurrent measurements, detrital zircon U-Pb data, and sandstone petrography for uppermost Oligocene-lower Miocene eolian sandstones from northern and central Argentina indicate the regional establishment of broadly westerly winds, consistent with a provenance record involving contributions from principally Phanerozoic rocks in the Andes rather than cratonic regions to the east. Exhumation of the Andean magmatic arc and retroarc fold-thrust belt resulted from shortening, thickening, and uplift of regions that today form the high-elevation hinterland, including: (a) the Western Cordillera, Puna plateau and Eastern Cordillera of northern Argentina at 22–26°S; and (b) the Principal Cordillera and Frontal Cordillera of western Argentina at 26–36°S. Independent structural and stratigraphic records for a latest Oligocene to early Miocene onset of major Andean shortening and enhanced sediment accumulation suggest that tectonically regulated topographic growth and rain shadow development were essential to the inception and persistence of eolian depositional conditions across the foreland basin.

CRediT authorship contribution statement

Daniel Starck: Writing - review & editing, Writing - original draft, Investigation, Conceptualization. **Tomas N. Capaldi:** Writing - review & editing, Writing - original draft, Methodology, Investigation, Funding acquisition. **Facundo Fuentes:** Writing - review & editing, Writing - original draft, Investigation, Conceptualization. **Brian K. Horton:** Writing - review & editing, Writing - original draft, Resources, Investigation, Funding acquisition, Conceptualization.

Declaration of competing interest

The authors declare the following financial interests/personal relationships which may be considered as potential competing interests:

Brian K. Horton reports financial support was provided by National Science Foundation. Tomas N. Capaldi reports financial support was provided by National Science Foundation. Tomas N. Capaldi reports financial support was provided by Geological Society of America. Tomas N. Capaldi reports financial support was provided by American Association of Petroleum Geologists.

Data availability

SUPPLEMENTARY DATA INCLUDED

Acknowledgments

This research was supported by U.S. National Science Foundation grants (EAR-1348031, EAR-191854, and EAR-2242878) awarded to B. K. Horton and T.N. Capaldi, and student research support from the Geological Society of America, American Association of Petroleum Geologists, and the Jackson School of Geosciences at the University of Texas at Austin awarded to T.N. Capaldi. The manuscript was improved by constructive reviews from Carlos Limarino and two anonymous reviewers. We thank the following for beneficial discussions: Gustavo Vergani, Andrés Boll, Chelsea Mackaman-Lofland, Kurt Constenius, Barbara Carrapa, Sarah George, Jaime Hirtz, Amanda Calle, Sebastian Ramirez, and Nicholas Regier.

Appendix A. Supplementary data

Supplementary data to this article can be found online at <https://doi.org/10.1016/j.jsames.2023.104758>.

References

- Allen, P.A., Verlander, J.E., Burgess, P.M., Audet, D.M., 2000. Jurassic giant erg deposits, flexure of the United States continental interior, and timing of the onset of Cordilleran shortening. *Geology* 28, 159–162.
- Amidon, W.A., Ciccioli, P.L., Marenssi, S.A., Limarino, C.O., Burch Fisher, G., Burbank, D., Kylander-Clark, A., 2016. U-Pb ages of detrital and volcanic zircons of the Toro Negro Formation, northwestern Argentina: Age, provenance and sedimentation rates. *J. S. Am. Earth Sci.* 70, 237–250. <https://doi.org/10.1016/j.james.2016.05.013>.
- Anderson, R.B., Long, S.B., Horton, B.K., Calle, A.Z., Ramirez, V., 2017. Shortening and structural architecture of the Andean fold-thrust belt of southern Bolivia (21°S): Implications for kinematic development and crustal thickening of the central Andes. *Geosphere* 13, 538–558. <https://doi.org/10.1130/GES01433.1>.
- Anderson, R.B., Long, S.P., Horton, B.K., Thomson, S.N., Calle, A.Z., Stockli, D.F., 2018. Orogenic wedge evolution of the central Andes, Bolivia (21°S): Implications for Cordilleran cyclicity. *Tectonics* 37, 3577–3609. <https://doi.org/10.1002/2018TC005132>.
- Arcila Gallego, P.A., 2010. Los depósitos sinorogénicos del sur de Mendoza y su relación con la faja plegada y corrida de Malargüe (35°-36° S), Mendoza, Argentina. [Ph.D. dissertation]. Universidad de Buenos Aires, 379 p.
- Astini, R.A., Benedetto, J.L., Vaccari, N.E., 1995. The early Paleozoic evolution of the Argentine Precordillera as a Laurentian rifted, drifted, and collided terrane: A geodynamic model. *Geol. Soc. Am. Bull.* 107, 253–273.
- Astini, R., Dávila, F., Gehrels, G., Mpodozis, C., 2009. Eolianites paleógenas del cinturón andino en el perfil de Pircas Negras, La Rioja, Argentina. XII Congreso Geológico Chileno, S10_004, 6 p.
- Balgord, E.A., 2017. Triassic to Neogene evolution of the south-central Andean arc determined by detrital zircon U-Pb and Hf analysis of Neuquén Basin strata, central Argentina (34°S–40°S). *Lithosphere* 9, 453–462. <https://doi.org/10.1130/L546.1>.
- Bjerrum, C.J., Dorsey, R.J., 1995. Tectonic controls on deposition of Middle Jurassic strata in a retroarc foreland basin, Utah–Idaho trough, western Interior, United States. *Tectonics* 14, 962–978.
- Boll, A., Hernández, R.M., 1986. Interpretación estructural del área Tres Cruces. *Bol. Inf. Pet.* 7, 2–14.
- Boll, A., Alonso, A., Fuentes, F., Vergara, M., Laffitte, G., Villar, H.J., 2014. In: Factores controlantes de las acumulaciones de hidrocarburos en el sector norte de la cuenca Neuquina, entre los ríos Diamante y Salado, Provincia de Mendoza, Argentina. Actas, Mendoza, Argentina, pp. 3–44.
- Bracco, A., Gómez, D., Diaz, I., 2015. Estratigrafía del miembro inferior de la Formación Culqui, Neógeno, San Juan, Argentina. XIV Congreso Geológico Chileno, Actas, pp. 707–710.
- Buelow, E.K., Suriano, J., Mahoney, J.B., Kimbrough, D.L., Mescua, J.F., Giambiagi, L.B., Hoke, G.D., 2018. Sedimentologic and stratigraphic evolution of the Cacheuta basin: Constraints on the development of the Miocene retroarc foreland basin, south-central Andes. *Lithosphere* 10, 366–391. <https://doi.org/10.1130/L709.1>.
- Calle, A.Z., Horton, B.K., Limachi, R., Stockli, D.F., Uzeda-Orellana, G.V., Anderson, R.B., Long, S.P., 2018. Cenozoic provenance and depositional record of the Sub-Andean foreland basin during growth of the central Andean fold-thrust belt, southern Bolivia. In: Zamora Valcance, G., McClay, K.R., Ramos, V.A. (Eds.), *Petroleum Basins and Hydrocarbon Potential of the Andes of Peru and Bolivia*: AAPG Memoir, 117, pp. 483–530. <https://doi.org/10.1306/13622132m1173777>.
- Calle, A.Z., Horton, B.K., García, R., Anderson, R.B., Stockli, D.F., Flraig, P.P., Long, S.P., 2023. Sediment dispersal and basin evolution during contrasting tectonic regimes along the western Gondwanan margin in the central Andes. *J. S. Am. Earth Sci.* 125 <https://doi.org/10.1016/j.james.2023.104286>.
- Candiani, J.C., Astini, R., Dávila, F., Collo, G., Ezpeleta, M., Alasino, P., Dahlquist, J., Carrizo, R., 2011. Hojas Geológicas 2969-18 y 2969-24, Famatina y Sañogasta, Provincia de La Rioja, 1:100,000, Boletín, 379. Servicio Geológico Minero Argentino, 163 p.
- Capaldi, T.N., Horton, B.K., McKenzie, N.R., Stockli, D.F., Odlum, M.L., 2017. Sediment provenance in contractional orogens: The detrital zircon record from modern rivers in the Andean fold-thrust belt and foreland basin of western Argentina. *Earth Planet Sci. Lett.* 479, 83–97. <https://doi.org/10.1016/j.epsl.2017.09.001>.
- Capaldi, T.N., George, S.W.M., Hirtz, J.A., Horton, B.K., Stockli, D.F., 2019. Fluvial and eolian sediment mixing during changing climate conditions recorded in Holocene Andean foreland deposits from Argentina (31–33°S). *Front. Earth Sci.* 7 <https://doi.org/10.3389/feart.2019.00298>.
- Capaldi, T.N., Horton, B.K., McKenzie, N.R., Mackaman-Lofland, C., Stockli, D.F., Ortiz, G., Alvarado, P., 2020. Neogene retroarc foreland basin evolution, sediment provenance, and magmatism in response to flat slab subduction, western Argentina. *Tectonics* 39. <https://doi.org/10.1029/2019TC005958>.
- Capaldi, T.N., McKenzie, N.R., Horton, B.K., Mackaman-Lofland, C., Colleps, C.L., Stockli, D.F., 2021. Detrital zircon record of Phanerozoic magmatism in the southern Central Andes. *Geosphere* 17, 876–897. <https://doi.org/10.1130/GES02346.1>.
- Carrapa, B., DeCelles, P.G., 2015. Regional exhumation and kinematic history of the central Andes in response to cyclical orogenic processes. *Geol. Soc. Am. Memoir*, 212, 201–213.
- Carrapa, B., Hauer, J., Schoenbohm, L., Strecker, M.R., Schmitt, A.K., Villanueva, A., Gómez, J.S., 2008. Dynamics of deformation and sedimentation in the northern Sierras Pampeanas: An integrated study of the Neogene Fiambalá basin, NW Argentina. *Geol. Soc. Am. Bull.* 120, 1518–1543.
- Carrapa, B., Bywater-Reyes, S., DeCelles, P., Mortimer, E., Gehrels, G.E., 2012. Late Eocene–Pliocene basin evolution in the Eastern Cordillera of northwestern Argentina (25°–26°S): regional implications for Andean orogenic wedge development. *Basin Res.* 23, 249–268. <https://doi.org/10.1111/j.1365-2117.2011.00519.x>.
- Cevallos, M., Milana, J.P., 1992. Sedimentología de un desierto eólico terciario (San Juan, Argentina). IV Reunión Argentina de Sedimentología. *Actas* 3, 121–128.
- Ciccioli, P.L., Limarino, C.O., Marenssi, S.A., 2005. Nuevas edades radimétricas para la Formación Toro Negro en la Sierra de Los Colorados, Sierras Pampeanas Noroccidentales, provincia de La Rioja. *Rev. Asoc. Geol. Argent.* 60, 251–254.
- Ciccioli, P., Limarino, C.O., Marenssi, S.A., Tedesco, A.M., Tripaldi, A., 2010. Estratigrafía de la cuenca de Vinchina (Terciario), Sierras Pampeanas, Provincia de La Rioja. *Rev. Asoc. Geol. Argent.* 66, 146–155.
- Ciccioli, P., Limarino, C.O., Marenssi, S.A., Tedesco, A.M., Tripaldi, A., 2011. Tectonosedimentary evolution of the La Troya and Vinchina depocenters (northern Bermejo Basin, Tertiary), La Rioja, Argentina. In: *Salfity, Marquillas, R.A. (Eds.), Cenozoic Geology of the Central Andes of Argentina*, pp. 91–110.
- Ciccioli, P.L., Limarino, C.O., Friedman, R., Marenssi, S.A., 2014a. New high precision U-Pb ages for the Vinchina Formation: implications for the stratigraphy of the Bermejo Andean foreland basin (La Rioja province, western Argentina). *J. S. Am. Earth Sci.* 56, 200–213. <https://doi.org/10.1016/j.james.2014.09.005>.
- Ciccioli, P.L., Marenssi, S.A., Limarino, C.O., 2014b. Petrology and provenance of the Toro Negro formation (Neogene) of the Vinchina broken-foreland basin (central Andes of Argentina). *J. S. Am. Earth Sci.* 49, 15–38.
- Ciccioli, P.L., Marenssi, S.A., Salvó Bernárdez, S.C., Limarino, C.O., 2023. The Oligocene – early Miocene erg in the western Andean basins: Patterns during the transition from eolian to fluvial sedimentation. *J. S. Am. Earth Sci.* 128 <https://doi.org/10.1016/j.james.2023.104456>.
- Coira, B.L., Davidson, J.D., Mpodozis, C., Ramos, V.A., 1982. Tectonic and magmatic evolution of the Andes of northern Argentina and Chile. *Earth Sci. Rev.* 18, 303–332. [https://doi.org/10.1016/0012-8252\(82\)90042-3](https://doi.org/10.1016/0012-8252(82)90042-3).
- Collo, G., Dávila, F.M., Nóbile, J., Astini, R.A., Gehrels, G., 2011. Clay mineralogy and thermal history of the Neogene Vinchina Basin, central Andes of Argentina: Analysis of factors controlling the heating conditions. *Tectonics* 30, TC4012. <https://doi.org/10.1029/2010TC002841>.
- Collo, G., Dávila, F.M., Teixeira, W., Nóbile, J.C., Sant'Anna, L.G., Carter, A., 2017. Isotopic and thermochronologic evidence of extremely cold lithosphere associated with a slab flattening in the Central Andes of Argentina. *Basin Res.* 29, 16–40. <https://doi.org/10.1111/bre.12163>.
- Coney, P.J., Evenchick, C.A., 1994. Consolidation of the American Cordilleras. *J. S. Am. Earth Sci.* 7, 241–262.
- Coutand, I., Carrapa, B., Deeken, A., Schmitt, A.K., Sobel, E.R., Strecker, M.R., 2006. Propagation of orographic barriers along an active range front: insights from sandstone petrography and detrital apatite fission-track thermochronology in the intramontane Angastaco basin, NW Argentina. *Basin Res.* 18, 1–26. <https://doi.org/10.1111/j.1365-2117.2006.00283.x>.
- Cristallini, E.O., Ramos, V.A., 2000. Thick-skinned and thin-skinned thrusting in the La Ramada fold and thrust belt: crustal evolution of the High Andes of San Juan, Argentina (32°SL). *Tectonophysics* 317, 205–235.
- Dahlquist, J.A., Alasino, P.H., Basei, M.A.S., Morales Cámera, M.M., Macchioli Grande, M., da Costa Campos Neto, M., 2018. Petrological, geochemical, isotopic, and geochronological constraints for the Late Devonian–Early Carboniferous magmatism in SW Gondwana (27–32°LS): an example of geodynamic switching. *Int. J. Earth Sci.* 107, 2575–2603. <https://doi.org/10.1007/s00531-018-1615-9>.
- Dávila, F.M., Astini, R.A., 2003. Las eolianitas de la Sierra de Famatina: Interacción paleoclima-tectónica en el antepaís fragmentado Andino central durante el Mioceno Medio? *Rev. Geol. Chile* 30, 187–204.
- Dávila, F.M., Astini, R.A., 2007. Cenozoic provenance history of synorogenic conglomerates in western Argentina (Famatina belt): Implications for Central Andean foreland development. *Geol. Soc. Am. Bull.* 119, 609–622.
- Dávila, F.M., Astini, R.A., Jordan, T.E., Kay, S.M., 2004. Early Miocene andesite conglomerates in the Sierra de Famatina, broken foreland region of western Argentina, and documentation of magmatic broadening in the south-central Andes. *J. S. Am. Earth Sci.* 17, 89–101. <https://doi.org/10.1016/j.james.2004.04.001>.
- DeCelles, P.G., Carrapa, B., Horton, B.K., Gehrels, G.E., 2011. Cenozoic foreland basin system in the central Andes of northwestern Argentina: Implications for Andean geodynamics and modes of deformation. *Tectonics* 30, TC6013. <https://doi.org/10.1029/2011TC002948>.
- DeCelles, P.G., Carrapa, B., Horton, B.K., McNabb, J., Gehrels, G.E., Boyd, J., Ducea, M.N., Kapp, P.A., 2015. The Miocene Arizaro Basin, central Andean hinterland: Response to partial lithosphere removal? *Geol. Soc. Am. Memoir* 212, 359–386.
- del Papa, C., Hongn, F., Powell, J., Payrola, P., Do Campo, M., Strecker, M., Petrinovic, I., Smith, A., Pereyra, R., 2013a. Middle Eocene–Oligocene broken-foreland evolution in the Andean Calchaquí Valley, NW Argentina: insights from stratigraphic, structural and provenance studies. *Basin Research* 25, 574–593.
- del Papa, C., Kirschbaum, A., Powell, J., Brod, A., Hongn, F., M, Pimentel, M., 2010. Sedimentological, geochemical and paleontological insights applied to continental omission surfaces: A new approach for reconstructing Eocene foreland basin in NW Argentina. *J. South Am. Earth Sci.* 29, 327–345. <https://doi.org/10.1016/j.james.2009.06.004>.
- del Papa, C., Payrola, P., Pingel, H., Hongn, F., Do Campo, M., Sobel, E.R., Lapiana, A., Cottle, J., Glodny, J., Strecker, M.R., 2021. Stratigraphic response to fragmentation of the Miocene Andean foreland basin, NW Argentina. *Basin Res.* 33, 2914–2937. <https://doi.org/10.1111/bre.12589>.
- del Papa, C., Hongn, F., Payrola, P., Powell, J., Deraco, V., Herrera, C., 2013b. Relaciones estratigráficas de las formaciones Quebrada de los Colorados y Angastaco (Paleógeno–Neógeno), valles Calchaquíes, Salta (Argentina): significado en el análisis de la cuenca del Grupo Payogastilla. *Lat. Am. J. Sedimentol. Basin Anal.* 20, 51–64.

- del Rey, A., Deckart, K., Arriagada, C., Martínez, F., 2016. Resolving the paradigm of the late Paleozoic–Triassic Chilean magmatism: Isotopic approach. *Gondwana Res.* 37, 172–181.
- Deri, M., Ciccioli, P.L., Amidon, W., Marenssi, S.A., 2019. Estratigrafía y edad máxima de deposición de la Formación Tambaréa en el Bolsón de Fiambalá, Catamarca. V Simposio del Mioceno – Pleistoceno del Centro y Norte de Argentina. Jujuy, Argentina, pp. 53–56.
- Deri, M., Ciccioli, P., Marenssi, S., Amidon, W., 2021. Revisión estratigráfica de la sucesión neógena en el Bolsón de Fiambalá, Sistema de Famatina, Catamarca, Argentina. *Rev. Asoc. Geol. Argent.* 78, 433–448.
- Dickinson, W.R., 1985. Interpreting provenance relations from detrital modes of sandstones. In: Zuffa (Ed.), Provenance of Arenites. NATO Advanced Studies Inst, Dordrecht, Netherlands, pp. 333–361.
- Echavarria, L., Hernández, R., Allmendinger, R., Reynolds, J., 2003. Subandean thrust and fold belt of northwestern Argentina: Geometry and timing of the Andean evolution: AAPG Bull. 87, 965–985.
- Fosdick, J.C., Carrapa, B., Ortiz, G., 2015. Faulting and erosion in the Argentine Precordillera during changes in subduction regime: Reconciling bedrock cooling and detrital records. *Earth Planet Sci. Lett.* 432, 73–83. <https://doi.org/10.1016/j.epsl.2015.09.041>.
- Fosdick, J.C., Reat, E.J., Carrapa, B., Ortiz, G., Alvarado, P.M., 2017. Retroarc basin reorganization and aridification during Paleogene uplift of the southern central Andes. *Tectonics* 36, 493–514. <https://doi.org/10.1002/2016TC004400>.
- Fuentes, F., Horton, B.K., 2020. The Andean foreland evolution of the Neuquén Basin: A discussion. In: Kietzmann, D., Folguera, A. (Eds.), Opening and Closure of the Neuquén Basin in the Southern Andes. Springer Earth System Sciences, pp. 341–370. https://doi.org/10.1007/978-3-030-29680-3_14.
- Fuentes, F., Horton, B.K., Starck, D., Boll, A., 2016. Structure and tectonic evolution of hybrid thick-and thin-skinned systems in the Malargüe fold-thrust belt, Neuquén basin, Argentina. *Geol. Mag.* 153, 1066–1084. <https://doi.org/10.1017/S0016756816000583>.
- Forque, G., González, P., Caballé, M., Pérez, L., Cardó, R., Godeas, M., Conde, A., Pucci, J.C., 2003. Hoja Geológica 3169-II, San José de Jáchal. Provincias de San Juan y La Rioja, 1:250,000, Boletín, 259. Instituto de Geología y Recursos Minerales, Servicio Geológico Minero Argentino, 77 p.
- Galli, C.I., Coira, B., Alonso, R., Reynolds, J., Matteini, M., Hauser, N., 2014. Tectonic controls on the evolution of the Andean Cenozoic foreland basin: Evidence from fluvial system variations in the Payogastilla Group, in the Calchaquí, Tonco and Amblayo Valleys, NW Argentina. *J. S. Am. Earth Sci.* 52, 234–259.
- Galli, C.I., Alonso, R.N., Coira, B.L., 2017. Integrated stratigraphy of the Cenozoic Andean foreland basin (northern Argentina). In: Ambrosino, G.A. (Ed.), Seismic and Sequence Stratigraphy and Integrated Stratigraphy. InTech Open Access, pp. 129–156. <https://doi.org/10.5772/intechopen.69985>.
- Galli, C.I., Alonso, R.N., Coira, B.L., 2023. Paleoenvironmental evolution of the Cenozoic foreland basin to intermontane basins in the Eastern Cordillera, North-Western Argentina. *J. S. Am. Earth Sci.* 130 <https://doi.org/10.1016/j.james.2023.104582>.
- Garzanti, E., Capaldi, T., Vezzoli, G., Limonta, M., Sosa, N., 2021. Transcontinental retroarc sediment routing controlled by subduction geometry and climate change (Central and Southern Andes, Argentina). *Basin Res.* 33, 3406–3437. <https://doi.org/10.1111/bre.12607>.
- Garzanti, E., Capaldi, T., Tripaldi, A., Zárate, M., Limonta, M., Vezzoli, G., 2022. Andean retroarc-basin dune fields and Pampean Sand Sea (Argentina): Provenance and drainage changes driven by tectonics and climate. *Earth Sci. Rev.* 231 <https://doi.org/10.1016/j.earscirev.2022.104077>.
- Gehrels, G.E., Valencia, V., Ruiz, J., 2008. Enhanced precision, accuracy, efficiency, and spatial resolution of U-Pb ages by laser ablation–multicollector–inductively coupled plasma–mass spectrometry. G-cubed 9. <https://doi.org/10.1029/2007GC001805>.
- Giambiagi, L.B., Alvarez, P.P., Godoy, E., Ramos, V.A., 2003. The control of pre-existing extensional structures on the evolution of the southern sector of the Aconcagua fold and thrust belt, southern Andes. *Tectonophysics* 369, 1–19.
- Giambiagi, L., et al., 2022. Crustal anatomy and evolution of a subduction-related orogenic system: Insights from the Southern Central Andes (22–35°S). *Earth Sci. Rev.* 232, 63–82. <https://doi.org/10.1016/j.earscirev.2022.104138>.
- Giambiagi, L., Mescua, J., Bechis, F., Tassara, A., Hoke, G., 2012. Thrust belts of the southern Central Andes: Along-strike variations in shortening, topography, crustal geometry, and denudation. *Geol. Soc. Am. Bull.* 124, 1339–1351.
- Grosso, S., López, R., Vergani, G., O’Leary, S., 2013. Reservorios carbonáticos naturalmente fracturados en el Yacimiento Caimancito (Formación Yacoraite), cuenca cretácica del noroeste Argentina. *Rev. Asoc. Geol. Argent.* 70, 53–69.
- Hain, M., Strecker, M., Bookhagen, B., Alonso, R., Pingel, H., Schmitt, A., 2011. Neogene to Quaternary broken foreland formation and sedimentation dynamics in the Andes of northwest Argentina (25°S). *Tectonics* 30, TC2006. <https://doi.org/10.1029/2010TC002703>.
- Hartley, A.J., Weissmann, G.S., Nichols, G.J., Warwick, G.L., 2010. Large distributive fluvial systems: Characteristics, distribution, and controls on development. *J. Sediment. Res.* 80, 167–183. <https://doi.org/10.2110/jsr.2010.016>.
- Haschke, M., Günther, A., Melnick, D., Echtler, H., Reutter, K.J., Scheuber, E., Oncken, O., 2006. Central and Southern Andean tectonic evolution inferred from arc magmatism. In: The Andes. Springer, Berlin Heidelberg, pp. 337–353.
- Hernández, R.M., Reynolds, J., Di Salvo, A., 1996. Análisis tectosedimentario y ubicación geocronológica del Grupo Orán en el Río Iruya: Boletín de Informaciones Petroleras. Tercera Epoca 45, 80–93.
- Hernández, R.M., Jordan, T.E., Farjat, A.D., Echavarria, L., Idleman, B.D., Reynolds, J.H., 2005. Age, distribution, tectonics, and eustatic controls of the Paranense and Caribbean marine transgressions in southern Bolivia and Argentina. *J. S. Am. Earth Sci.* 19, 495–512.
- Hervé, F., Fanning, C.M., Calderon, M., Mpodozis, C., 2014. Early Permian to Late Triassic batholiths of the Chilean Frontal Cordillera (28–31°S): SHRIMP U-Pb zircon ages and Lu-Hf and O isotope systems. *Lithos* 187, 436–446.
- Horton, B.K., 1999. Erosional control on the geometry and kinematics of thrust belt development in the central Andes. *Tectonics* 18, 1292–1304.
- Horton, B.K., 2018a. Tectonic regimes of the central and southern Andes: Responses to variations in plate coupling during subduction. *Tectonics* 37, 402–429. <https://doi.org/10.1002/2017TC004624>.
- Horton, B.K., 2018b. Sedimentary record of Andean mountain building. *Earth Sci. Rev.* 178, 279–309. <https://doi.org/10.1016/j.earscirev.2017.11.025>.
- Horton, B.K., DeCelles, P.G., 2001. Modern and ancient fluvial megafans in the foreland basin system of the central Andes, southern Bolivia: implications for drainage network evolution in fold-thrust belts. *Basin Res.* 13, 43–63.
- Horton, B.K., Fuentes, F., 2016. Sedimentary record of plate coupling and decoupling during growth of the Andes. *Geology* 44, 647–650. <https://doi.org/10.1130/G37918.1>.
- Horton, B.K., Fuentes, F., Boll, A., Starck, D., Ramirez, S.G., Stockli, D.F., 2016. Andean stratigraphic record of the transition from backarc extension to orogenic shortening: A case study from the northern Neuquén Basin, Argentina. *J. S. Am. Earth Sci.* 71, 17–40. <https://doi.org/10.1016/j.james.2016.06.003>.
- Horton, B.K., Capaldi, T.N., Mackaman-Lofland, C., Perez, N.D., Bush, M.A., Fuentes, F., Constenius, K.N., 2022a. Broken foreland basins and the influence of subduction dynamics, tectonic inheritance, and mechanical triggers. *Earth Sci. Rev.* 234 <https://doi.org/10.1016/j.earscirev.2022.104193>.
- Horton, B.K., Capaldi, T.N., Perez, N.D., 2022b. The role of flat slab subduction, ridge subduction, and tectonic inheritance in Andean deformation. *Geology* 50, 1007–1012. <https://doi.org/10.1130/G50094.1>.
- Irigoyen, M.V., Buchan, K.L., Brown, R.L., 2000. Magnetostratigraphy of Neogene Andean foreland-basin strata, lat 33°S, Mendoza Province, Argentina. *Geol. Soc. Am. Bull.* 112, 803–816.
- Johnson, N.M., Jordan, T.E., Johnsson, P.A., Naeser, C.W., 1986. Magnetic polarity stratigraphy, age and tectonic setting of fluvial sediments in an eastern Andean foreland basin, San Juan Province, Argentina. In: Allen, P.A., Homewood, P. (Eds.), Foreland Basins, vol. 8. International Association of Sedimentologists, Special Publication, pp. 63–75.
- Jones, R.E., Kirstein, L.A., Kasemann, S.A., Litvak, V.D., Poma, S., Alonso, R.N., Hinton, R., 2016. The role of changing geodynamics in the progressive contamination of Late Cretaceous to Late Miocene arc magmas in the southern Central Andes. *Lithos* 262, 169–191. <https://doi.org/10.1016/j.lithos.2016.07.002>.
- Jordan, T.E., Alonso, R.N., 1987. Cenozoic stratigraphy and basin tectonics of the Andes Mountains, 20°–28° south latitude. *AAPG Bull.* 71, 49–64.
- Jordan, T.E., Rutty, P., McRae, L., Beer, J., Tabbutt, K., Damanti, J., 1990. Magnetic polarity of the Miocene Rio Azul section, Precordillera thrust belt, San Juan Province, Argentina. *J. Geol.* 98, 519–539.
- Jordan, T.E., Allmendinger, R.W., Damanti, J.F., Drake, R.E., 1993. Chronology of motion in a complete thrust belt: The Precordillera, 30–31°S, Andes Mountains. *J. Geol.* 101, 135–156.
- Jordan, T.E., Tamm, V., Figueroa, G., Flemings, P.B., Richards, D., Tabbutt, K., Cheatham, H., 1996. Development of the Miocene Manantiales foreland basin, Principal Cordillera, San Juan, Argentina. *Rev. Geol. Chile* 23, 43–79.
- Jordan, T.E., Schlunegger, F., Cardozo, N., 2001. Unsteady and spatially variable evolution of the Neogene Andean Bermejo foreland basin, Argentina. *J. S. Am. Earth Sci.* 14, 775–798.
- Kay, S.M., Mpodozis, C., Ramos, V.A., Munizaga, F., 1991. Magma source variations for mid-late Tertiary magmatic rocks associated with a shallowing subduction zone and a thickening crust in the central Andes (28 to 33°S). In: Harmon, R.S., Rapela, C.W. (Eds.), Andean Magmatism and its Tectonic Setting, vol. 265. Geological Society of America Special Paper, pp. 113–137.
- Kleiman, L.E., Japas, M.S., 2009. The Choiyoi volcanic province at 34°S–36°S (San Rafael, Mendoza, Argentina): Implications for the Late Paleozoic evolution of the southwestern margin of Gondwana. *Tectonophysics* 473, 283–299.
- Kley, J., Monaldi, C.R., 2002. Tectonic inversion in the Santa Barbara system of the central Andean foreland thrust belt, northwestern Argentina. *Tectonics* 21, 1061. <https://doi.org/10.1029/2002TC002003>.
- Kraemer, B., Adelmann, D., Alten, M., Schnurr, W., Erpenstein, K., Kiefer, E., van den Bogaard, P., Görler, K., 1999. Incorporation of the Paleogene foreland into the Neogene Puna plateau: The Salar de Antofalla area, NW Argentina. *J. S. Am. Earth Sci.* 12 (2), 157–182.
- Leier, A.L., DeCelles, P.G., Pelletier, J.D., 2005. Mountains, monsoons, and megafans. *Geology* 33, 289–292. <https://doi.org/10.1130/G21228.1>.
- Levina, M., Horton, B.K., Fuentes, F., Stockli, D.F., 2014. Cenozoic sedimentation and exhumation of the foreland basin system preserved in the Precordillera thrust belt (31–32°S), southern central Andes, Argentina: Tectonics 33, 1659–1680. <https://doi.org/10.1029/2013TC003424>.
- Liebrand, D., de Bakker, A.T., Beddoe, H.M., Wilson, P.A., Bohaty, S.M., Ruessink, G., Pálikie, H., Batenburg, S.J., Hilgen, F.J., Hodell, D.A., Huck, C.E., 2017. Evolution of the early Antarctic ice ages. *Proc. Natl. Acad. Sci.* 114, 3867–3872.
- Limarino, C.O., Net, L., Gutierrez, P., Barreda, V., Caselli, A., Ballent, S., 2000. Lithostratigraphical definition of the Cienega del Río Huaco Formation (Cretaceous), Precordillera central, San Juan, Argentina. *Rev. Asoc. Geol. Argent.* 55, 83–89.
- Limarino, C., Tripaldi, A., Marenssi, S., Net, L., Re, G., Caselli, A., 2001. Tectonic control on the evolution of the fluvial systems of the Vinchina Formation (Miocene), northwestern Argentina. *J. S. Am. Earth Sci.* 14, 751–762.
- Limarino, C.O., Fauqué, L.A., Cardó, R., Gagliardo, M.L., Escoteguy, L., 2002. La faja volcánica miocena de la Precordillera septentrional. *Rev. Asoc. Geol. Argent.* 57, 289–304.

- Limarino, C.O., Ciccioli, P.L., Krapovickas, V., Benedito, L.D., 2016. Estratigrafía de las sucesiones mesozoicas, paleógenas y neógenas de las quebradas Santo Domingo y El Peñón (Precordillera septentrional riojana). Rev. Asoc. Geol. Argent. 73, 301–318.
- Mackaman-Lofland, C., Horton, B.K., Fuentes, F., Constenius, K.N., Stockli, D.F., 2019. Mesozoic to Cenozoic retroarc basin evolution during changes in tectonic regime, southern Central Andes (31°–33°S): Insights from zircon U-Pb geochronology. J. S. Am. Earth Sci. 89, 299–318. <https://doi.org/10.1016/j.jsames.2018.10.004>.
- Mackaman-Lofland, C., Horton, B.K., Fuentes, F., Constenius, K.N., Ketcham, R.A., Capaldi, T.N., Stockli, D.F., Ammirati, J.B., Alvarado, P., Orozco, P., 2020. Andean mountain building and foreland basin evolution during thin- and thick-skinned Neogene deformation (32°–33°S). Tectonics 39. <https://doi.org/10.1029/2019TC005838>.
- Mackaman-Lofland, C., Horton, B.K., Ketcham, R.A., McQuarrie, N., Fosdick, J.C., Fuentes, F., Constenius, K.N., Capaldi, T.N., Stockli, D.F., Alvarado, P., 2022. Causes of variable shortening and tectonic subsidence during changes in subduction: Insights from flexural thermokinematic modeling of the Neogene southern central Andes (28°–30°S). Tectonics 41. <https://doi.org/10.1029/2022TC007334>.
- Maloney, K.T., Clarke, G.L., Klepeis, K.A., Quevedo, L., 2013. The Late Jurassic to present evolution of the Andean margin: Drivers and the geological record. Tectonics 32, 1049–1065. <https://doi.org/10.1029/tect.20067>.
- Marengó, H.G., Forasiepi, A., Chiesa, J.O., 2019. Estratigrafía, paleontología y paleoambientes del Mioceno temprano y medio del centro y norte de Argentina. *Opera Lilloana* 52, 16–108.
- Melchor, R.N., Buchwaldt, R., Bowring, S., 2013. Late Eocene date for Late Triassic bird tracks. Nature 495, E1–E2.
- Milana, J.P., 1993. Estratigrafía de eolianitas en la zona de Jáchal-Huaco, Precordillera de San Juan. Rev. Asoc. Geol. Argent. 48, 283–298.
- Milana, J.P., Cevallos, M., Zavattieri, A.M., Pramparo, M., Papu, H.O., 1993. La secuencia terciaria de Pachaco: Sedimentología, edad, correlaciones y significado paleogeográfico. XIII Congreso Geológico Argentino, Actas, vol. 1 226–234.
- Montgomery, D.R., Balco, G., Willett, S.D., 2001. Climate, tectonics, and the morphology of the Andes. *Geology* 29, 579–582.
- Moreno, J.A., Dahlquist, J.A., Morales Cámera, M.M., Alasino, P.H., Larrovere, M.A., Basel, M.A.S., Galindo, C., Zandomeni, P.S., Rocher, S., 2020. Geochronology and geochemistry of the Tabaquito batholith (Frontal Cordillera, Argentina): geodynamic implications and temporal correlations in the SW Gondwana margin. *J. Geol. Soc. London* 177, 455–474. <https://doi.org/10.1144/jgs2019-062>.
- Mpodozis, C., Kay, S.M., 1992. Late Paleozoic to Triassic evolution of the Gondwana margin: Evidence from Chilean Frontal Cordilleran batholiths (28 to 31°S). *Geol. Soc. Am. Bull.* 104, 999–1014.
- Oliveros, V., González, J., Vargas, M.E., Vásquez, P., Rossel, P., Creixell, C., Sepúlveda, F., Bastias, F., 2018. The early stages of the magmatic arc in the southern central Andes. In: *The Evolution of the Chilean-Argentinean Andes*. Springer, Cham, pp. 165–190.
- Otamendi, J.E., Dueca, M.N., Cristofolini, E.A., Tibaldi, A.M., Camilletti, G.C., Bergantz, G.W., 2017. U-Pb ages and Hf isotope compositions of zircons in plutonic rocks from the central Famatinian arc, Argentina. *J. S. Am. Earth Sci.* 76, 412–426.
- Payrola, P., del Papa, C., Aramayo, A., Pingel, H., Hongn, F., Sobel, E.R., Zeilinger, G., Strecker, M.R., Zapata, S., Cottle, J., Salado Paz, N., Glodny, J., 2020. Episodic out-of-sequence deformation promoted by Cenozoic fault reactivation in NW Argentina. *Tectonophysics* 776. <https://doi.org/10.1016/j.tecto.2019.228276>.
- Pérez, D.J., 1995. Estudio geológico del Cordon del Espinacito y regiones adyacentes, provincia de San Juan. [Ph.D. dissertation]. Universidad de Buenos Aires, 262 p.
- Pérez, D.J., 2001. Tectonic and unroofing history of Neogene Manantiales foreland basin deposits, Cordillera Frontal (32°30'S), San Juan Province, Argentina. *J. S. Am. Earth Sci.* 14, 693–705. [https://doi.org/10.1016/S0895-9811\(01\)00071-2](https://doi.org/10.1016/S0895-9811(01)00071-2).
- Pfuhl, H.A., McCave, I.N., 2005. Evidence for late Oligocene establishment of the Antarctic Circumpolar Current. *Earth Planet. Sci. Lett.* 235, 715–728.
- Pinto, L., Alarcón, P., Morton, A., Naipauer, M., 2018. Geochemistry of heavy minerals and U-Pb detrital zircon geochronology in the Manantiales Basin: Implications for Frontal Cordillera uplift and foreland basin connectivity in the Andes of central Argentina. *Palaeogeogr. Palaeoclimatol. Palaeoecol.* 492, 104–125. <https://doi.org/10.1016/j.palaeo.2017.12.017>.
- Plonka, Z.C., Capaldi, T.N., Odium, M.L., Mackaman-Lofland, C., Ortiz, G., Alvarado, P., 2023. Along-strike tectonic evolution of the Neogene Bermijo foreland basin and Eastern Precordillera thrust front, Argentina (30–32°S). *J. S. Am. Earth Sci.* <https://doi.org/10.1016/j.jsames.2023.104521>.
- Ramos, V.A., 1996. Evolución tectónica de la Alta Cordillera de Mendoza. In: Ramos, V. A. (Ed.), *Geología de la Región del Aconcagua, Provincias de San Juan y Mendoza, República Argentina*. Dirección Nacional del Servicio Geológico, Anales 24 (12), pp. 447–460.
- Ramos, V.A., 1999. Los depósitos sinorogénicos terciarios de la región andina. In: Caminos, R. (Ed.), *Geología Argentina*. Instituto de Geología y Recursos Naturales, Anales 29, pp. 651–682.
- Ramos, V.A., 2004. Cuyana, an exotic block to Gondwana: Review of a historical success and the present problems. *Gondwana Res.* 7, 1009–1026.
- Ramos, V.A., Cegarra, M.L., Cristallini, E., 1996. Cenozoic tectonics of the High Andes of west-central Argentina (30°–36°S latitude). *Tectonophysics* 259, 185–200.
- Ramos, V.A., Cristallini, E.O., Perez, D.J., 2002. The Pampean flat-slab of the central Andes. *J. S. Am. Earth Sci.* 15, 59–78.
- Rapela, C.W., Verdecchia, S.O., Casquet, C., Pankhurst, R.J., Baldo, E.G., Galindo, C., Murra, J.A., Dahlquist, J.A., Fanning, C.M., 2016. Identifying Laurentian and SW Gondwana sources in the Neoproterozoic to early Paleozoic metasedimentary rocks of the Sierras Pampeanas: Paleogeographic and tectonic implications. *Gondwana Res.* 32, 193–212.
- Rapela, C.W., Pankhurst, R.J., Casquet, C., Dahlquist, J.A., Fanning, C.M., Baldo, E.G., Galindo, C., Alasino, P.H., Ramacciotti, C.D., Verdecchia, S.O., Murra, J.A., 2018. A review of the Famatinian Ordovician magmatism in southern South America: evidence of lithosphere reworking and continental subduction in the early proto-Andean margin of Gondwana. *Earth Sci. Rev.* 187, 259–285.
- Reat, E.J., Fosdick, J.C., 2018. Basin evolution during Cretaceous-Oligocene changes in sediment routing in the Eastern Precordillera, Argentina. *J. S. Am. Earth Sci.* 84, 422–443.
- Reynolds, J.H., Jordan, T.E., Johnson, N.M., Damanti, J.F., Tabbutt, K.D., 1990. Neogene deformation of the flat-subduction segment of the Argentine-Chilean Andes: Magnetostratigraphic constraints from Las Juntas, La Rioja province, Argentina. *Geol. Soc. Am. Bull.* 102, 1607–1622.
- Reynolds, J.H., Hernández, R.M., Galli, C.I., Idleman, B.D., 2001. Magnetostratigraphy of the Quebrada La Porcelana section, Sierra de Ramos, Salta Province, Argentina: Age limits for the Neogene Orán Group and uplift of the southern Sierras Subandinas. *J. S. Am. Earth Sci.* 14, 681–692.
- Rodríguez, M.P., Charrier, R., Brichau, S., Carretier, S., Farías, M., de Parseval, P., Ketcham, R.A., 2018. Latitudinal and longitudinal patterns of exhumation in the Andes of north-central Chile. *Tectonics* 37, 2863–2886. <https://doi.org/10.1029/2018TC004997>.
- Rosario, J., Hernández, J., Hernández, R., Jordan, T., 2008. Evolución tectono-sedimentaria durante el Terciario en la provincia de Jujuy. In: Coria, B., Zappettini, E. (Eds.), *Geología y Recurso Naturales de la Provincia de Jujuy*, Relatorio del XVII Congreso Argentino, pp. 263–285.
- Safipour, R., Carrapa, B., DeCelles, P.G., Thomson, S.N., 2015. Exhumation of the Precordillera and northern Sierras Pampeanas and along-strike correlation of the Andean orogenic front, northwestern Argentina. In: *Geol. Soc. Am. Memoir*, 212, pp. 181–199.
- Sato, A.M., Llambías, E.J., Basel, M.A., Castro, C.E., 2015. Three stages in the Late Paleozoic to Triassic magmatism of southwestern Gondwana, and the relationships with the volcanic events in coeval basins. *J. S. Am. Earth Sci.* 63, 48–69.
- Servicio Geológico Minero (SEGE MAR), 1999. *Geología Argentina: 1:3,000,000, digital version. SEGE MAR CD-ROM*, Buenos Aires, Argentina.
- Servicio Geológico Minero (SEGE MAR), 2012. Sistema de Información Geográfica del Servicio Geológico Minero Argentino. Buenos Aires, Argentina. sigam.segemar.gov.ar.
- Servicio Nacional de Geología y Minería (Sernageomin), 2003. *Mapa Geológico de Chile: 1:1,000,000, digital version. Sernageomin Publicación Geológica Digital 4*.
- Siks, B.C., Horton, B.K., 2011. Growth and fragmentation of the Andean foreland basin during eastward advance of fold-thrust deformation, Puna plateau and Eastern Cordillera, northern Argentina. *Tectonics* 30, TC6017. <https://doi.org/10.1029/2011TC002944>.
- Starck, D., 2011. Cuenca Cretácica-Paleógena del noroeste Argentina. In: *Congreso de Exploración y Desarrollo de Hidrocarburos, Simposio Cuencas Argentinas*, vol. 8. Instituto Argentino del Petróleo y el Gas, Mar del Plata, Argentina, pp. 407–453.
- Starck, D., Anzótegui, L., 2001. The late Miocene climatic change—persistence of a climatic signal through the orogenic stratigraphic record in northwestern Argentina. *J. S. Am. Earth Sci.* 14, 763–774.
- Starck, D., Schulz, A., 2017. Corte estructural del Sierras Subandinas a los 22.5°S: Aspectos estratigráficos, estructurales y geología del petróleo de la cuenca paleozoica del noreste. XX Congreso Geológico Argentino. Tucumán, Argentina. Guía de campo excursión geológica. 35 p.
- Starck, D., Vergani, G., 1996. Desarrollo tecto-sedimentario del Cenozoico en el sur de la Provincia de Salta-Argentina. XIII Congreso Geológico Argentino y III Congreso de Exploración de Hidrocarburos, vol. 1, Buenos Aires, Argentina, pp. 433–452. In: .
- Starck, D., Delupi, R., Ghidina, M., Strada, N., 2018. Formación Tranquitas y “Terciario Subandino”, Yacimiento Campo Durán. In: Schiuma, M., Hinterwimmer, G., Vergani, G. (Eds.), *Rocas Reservorio de las Cuencas Productivas de Argentina. Mendoza, Argentina*, pp. 1036–1048.
- Steinhorsdottir, M., et al., 2021. The Miocene: The future of the past. *Paleoceanography and Paleoclimatology* 36. <https://doi.org/10.1029/2020PA004037>.
- Stevens Goddard, A.L., Carrapa, B., 2018. Using basin thermal history to evaluate the role of Miocene–Pliocene flat-slab subduction in the southern Central Andes (27°S–30°S). *Basin Res.* 30, 564–585. <https://doi.org/10.1111/bre.12265>.
- Stevens Goddard, A.L., Carrapa, B., Aciar, R., 2020. Recognizing drainage reorganization in the stratigraphic record of the Neogene foreland basin of the Central Andes. *Sediment. Geol.* 405 <https://doi.org/10.1016/j.sedgeo.2020.105704>.
- Strecker, M.R., Alonso, R.N., Bookhagen, B., Carrapa, B., Hilley, G.E., Sobel, E.R., Trauth, M.H., 2007. Tectonics and climate of the southern Central Andes. *Annu. Rev. Earth Planet. Sci.* 35, 747–787.
- Suriano, J., Mardonez, D., Mahoney, J.B., Mescua, J.F., Giambiagi, L.B., Kimbrough, D., Lossada, A., 2017. Uplift sequence of the Andes at 30°S: Insights from sedimentology and U/Pb dating of synorogenic deposits. *J. S. Am. Earth Sci.* 75, 11–34.
- Suriano, J., Lossada, A.C., Mahoney, J.B., Tedesco, A.M., Limarino, C.O., Giambiagi, L.B., Mazzitelli, M.A., Mescua, J.F., Lothari, L., Quiroga, R., 2023. The southern extension of the Eocene Andean orogeny: New sedimentary record of the foreland basin in the southern Central Andes at 32°S. *Basin Res.* <https://doi.org/10.1111/bre.12803>.
- Tabbutt, K.D., 1990. Temporal constraints on the tectonic evolution of the Sierra de Famatina, northwestern Argentina, using the fission-track method to date tuffs interbedded in synorogenic clastic sedimentary strata. *J. Geol.* 98, 557–566.
- Tamagno, I., Suriano, J., Schenckman, L.J., Mardonez, D., 2018. Sedimentology of the Cuculí Formation at the río Francia creek, San Juan. *Rev. Asoc. Geol. Argent.* 75, 346–358.
- Tripladi, A., 2012. La Formación Vallecito como ejemplo de sedimentación eólica cenozoica de la cuenca andina del Noroeste Argentino: Paleoambientes y

- consideraciones estratigráficas y paleoclimáticas. *Anales Academia Nacional de Ciencias Exactas, Física y Naturales* 64, 55–71.
- Tripaldi, A., Ciccioli, P.L., Alonso, M.S., Forman, S.L., 2010. Petrography and geochemistry of late Quaternary dune fields of western Argentina: Provenance of eolian materials in southern South America. *Aeolian Research* 2, 33–48.
- Tripaldi, A., Limarino, C., 2005. Vallecito Formation (Miocene): The evolution of an eolian system in an Andean foreland basin (northwestern Argentina). *J. S. Am. Earth Sci.* 19, 343–357.
- Tripaldi, A., Net, L., Limarino, C.O., Marenssi, S., Re, G., Caselli, A., 2001. Paleoambientes sedimentarios y procedencia de la Formación Vinchina, Mioceno, noroeste de la provincia de La Rioja. *Rev. Asoc. Geol. Argent.* 56, 443–465.
- Vandervoort, D.S., Jordan, T.E., Zeitler, P.K., Alonso, R.N., 1995. Chronology of internal drainage development and uplift, southern Puna Plateau, Argentine central Andes. *Geology* 23, 145–148.
- Vergés, J., Ramos, E., Seward, D., Busquets, P., Colombo, F., 2001. Miocene sedimentary and tectonic evolution of the Andean Precordillera at 31°S, Argentina. *J. S. Am. Earth Sci.* 14, 735–750. [https://doi.org/10.1016/S0895-9811\(01\)00070-0](https://doi.org/10.1016/S0895-9811(01)00070-0).
- Viale, M., Bianchi, E., Cara, L., Ruiz, L.E., Villalba, R., Pitte, P., 2019. Contrasting climates at both sides of the Andes in Argentina and Chile. *Front. Environ. Sci.* 7 <https://doi.org/10.3389/fenvs.2019.00069>.
- Vizán, H., Geuna, S., Melchor, R., Bellosi, E.S., Lagorio, S.L., Vásquez, G., Japas, M.S., Ré, G., Do Campo, M., 2013. Geological setting and paleomagnetism of the Eocene red beds of Laguna Brava Formation (Quebrada Santo Domingo, northwestern Argentina). *Tectonophysics* 583, 105–123.
- Voss, R., 2002. Cenozoic stratigraphy of the southern Salar de Antofalla region, northwestern Argentina. *Rev. Geol. Chile* 29, 167–189.
- Yrigoyen, M., 1993. Los depósitos sinorogénicos terciarios. In: Ramos, V.A. (Ed.), *Geología y Recursos Naturales de Mendoza, XII Congreso Geológico Argentino y II Congreso de Exploración de Hidrocarburos*, vol. 1 (11), pp. 123–148.
- Zachos, J.C., Flower, B.P., Paul, H., 1997. Orbitally paced climate oscillations across the Oligocene/Miocene boundary. *Nature* 388, 567–570.
- Zambrano, O., Rapalini, A.E., Dávila, F.M., Astini, R.A., Spagnuolo, C.M., 2011. Magnetostratigraphy and paleomagnetism of early and middle Miocene synorogenic strata: basement partitioning and minor block rotation in Argentine broken foreland. *Int. J. Earth Sci.* 100, 591–602.